



Characteristics of debris flow prone watersheds and triggering rainstorms following the Tadpole Fire, New Mexico, USA

Luke A. McGuire¹, Francis K. Rengers², Ann M. Youberg³, Alexander N. Gorr¹, Olivia J. Hoch², Rebecca Beers³, Ryan Porter⁴

5 ¹Department of Geosciences, University of Arizona, Tucson, Arizona, 85721, USA

²U.S. Geological Survey, Golden, Colorado, 80401, USA

³Arizona Geological Survey, The University of Arizona, Tucson, AZ, 85721, USA

⁴School of Earth and Sustainability, Northern Arizona University, Flagstaff, AZ, 86011, USA

10 *Correspondence to:* Luke A. McGuire (lmcguire@arizona.edu)

Abstract. Moderate and high severity fires promote increases in runoff and erosion, leading to a greater likelihood of extreme geomorphic responses, including debris flows. In the first several years following fire, the majority of debris flows initiate when runoff rapidly entrains sediment on steep slopes. From a hazard perspective, it is important to be able to anticipate when and where watershed responses will be dominated by debris flows rather than flood flows. Rainfall intensity averaged over a 15-minute duration, I_{15} , in particular, has been identified as a key predictor of debris flow likelihood. Developing effective warning systems and predictive models for post-fire debris flow hazards therefore relies on high-temporal resolution rainfall data at the time debris flows initiate. In this study, we documented the geomorphic response of a series of watersheds following a wildfire in western New Mexico, USA, with an emphasis on constraining debris flow timing within rainstorms to better characterize debris flow-triggering rainfall intensities. We estimated temporal changes in soil hydraulic properties and ground cover in areas burned at different severities over 2+ years to offer explanations for observed differences in spatial and temporal patterns in debris flow activity. We observed 16 debris flows, all of which initiated during the first several months following the fire. The average recurrence interval of the debris flow-triggering I_{15} is 1.3 years, which highlights the susceptibility of recently burned watersheds to runoff-generated debris flows in this region. All but one of the debris flows initiated in watersheds burned primarily at moderate or high soil burn severity. Since soil hydraulic properties appeared to be relatively resilient to burning, we attribute reduced debris flow activity at later times to decreases in the fraction of bare ground. Results provide additional constraints on the rainfall characteristics that promote post-fire debris flow initiation in a region where fire size and severity have been increasing.



30 **1 Introduction**

Changes to canopy and ground cover, soil hydraulic properties, and soil erodibility following fire can promote order-of-magnitude increases in runoff and sediment yield relative to similar unburned areas (Robichaud et al., 2016). As a consequence, burned watersheds are more susceptible to extreme responses during rainstorms, including debris flows (Wells, 1987; Kean et al., 2011). Post-fire debris flows (PFDFs) often initiate in the first several years following fire when runoff rapidly entrains
35 sediment (DeGraff et al., 2015; Parise and Cannon, 2012). PFDFs that initiate from surface water runoff have been documented in a range of geographic and climate regions (Wall et al., 2020; Nyman et al., 2011; Gabet and Bookter, 2008; Larsen et al., 2006; Raymond et al., 2020; Kean et al., 2011; McGuire et al., 2021; Esposito et al., 2023; García-Ruiz et al., 2013; Diakakis et al., 2023; Conedera et al., 2003). Debris flows pose a hazard to people and infrastructure downstream of burned areas (Kean et al., 2019; Lancaster et al., 2021) and may also impact water quality (Langhans et al., 2016) and fish habitat (Smith et al.,
40 2021). As the western USA, a region susceptible to PFDF hazards (Staley et al., 2020), experiences increases in both area burned (Holden et al., 2018) and the frequency of extreme precipitation (Kirchmeier-Young and Zhang, 2020), improving our ability to identify when and where debris flows are most likely to initiate within burned areas will help to better assess hazards and prioritize mitigation efforts.

45 One component of PFDF hazard assessments includes identifying watersheds that are most susceptible to debris flows (Tillery and Matherne, 2012). It is important to identify watersheds that are susceptible to debris flows since the high sediment concentration in debris flows changes their flow behaviour, resulting in coarse-grained flow fronts with peak discharges and flow depths that can exceed those expected from water-dominated flows (Kean et al., 2016). Empirical models designed to predict PFDF likelihood based on the physiographic characteristics of a burned watershed illustrate that likelihood increases
50 with metrics related to soil burn severity, watershed steepness, and rainfall intensity (Cannon et al., 2010; Staley et al., 2017). Rainfall intensities averaged over relatively short durations (i.e., ≤ 30 min) are the best predictors of PFDF response (Staley et al., 2013). Soil burn severity is relevant since the impacts of fire on vegetation, ground cover, and soil properties, particularly soil erodibility (Vieira et al., 2015), are often most accentuated in areas burned at moderate or high severity. Such impacts may include reductions in canopy interception (Stoof et al., 2012), water storage in litter and duff layers (Robichaud et al., 2016),
55 surface roughness (Stoof et al., 2015), soil infiltration capacity (Ebel and Martin, 2017), and critical thresholds for sediment entrainment (Moody et al., 2005). Areas burned at moderate or high severity are therefore particularly susceptible to infiltration-excess overland flow during short-duration, high intensity bursts of rainfall, which can lead to extreme erosion and debris flow responses. Post-fire observations that identify which watersheds produce PFDFs are critical for improving conceptual and empirical models for PFDF likelihood.

60

In addition to identifying watersheds that are susceptible to debris flows, an additional element of many PFDF hazard assessments involves estimating the rainfall characteristics likely to produce debris flows (Staley et al., 2017). Rainfall



intensity-duration (ID) thresholds, which have traditionally been defined regionally based on inventories of rainstorms that have produced debris flows, are a practical and reliable approach for determining the rainstorms likely to produce PFDFs (Cannon et al., 2008; Staley et al., 2013; Raymond et al., 2020; Esposito et al., 2023; McGuire and Youberg, 2020). The empirical models developed by Staley et al. (2017) using data from the western USA can also be used to define a watershed-specific rainfall ID threshold based on soil, terrain, and burn severity characteristics. Regardless of the methodology used to define a rainfall ID threshold, a key source of uncertainty involves the unknown timing of debris flows within rainstorms and the implications for determining debris flow triggering rainfall intensities. Debris flows may initiate in response to rainfall intensities that are substantially lower than the peak rainfall intensity observed during a rainstorm (Staley et al., 2013; Raymond et al., 2020). However, in lieu of real-time measurements that constrain the timing of debris flows within a storm, a common assumption is that the rainfall intensity associated with debris flow initiation is equal to the most intense rainfall observed during the debris flow producing storm. Developing rainfall ID thresholds assuming that peak rainstorm intensity and debris flow triggering intensities are equal can result in overestimates of ID thresholds (Raymond et al., 2020), which could lead to an increase in false negatives (i.e., rainfall remains below the threshold, but a debris flow is observed). Observations that constrain the timing of PFDFs within rainstorms are therefore especially valuable for improving estimates of the rainfall intensities and durations required to produce debris flow responses.

Past work demonstrates a number of similarities in the factors that promote PFDF initiation across geographic and climate regions, including the importance of rainfall intensity over durations less than 30 minutes (Raymond et al., 2020; Friedman and Santi, 2019; Kean et al., 2011; Staley et al., 2013; Esposito et al., 2023) and presence of steep slopes burned at moderate or high soil burn severity (Cannon et al., 2010; Staley et al., 2017), but it also highlights key differences. Site-specific fire impacts, in combination with local terrain properties and rainfall climatology, modulate a recently burned landscapes' response to rainfall, with implications for debris flow initiation. For example, dry ravel is an important driver of PFDFs in the Transverse Ranges of southern California (DiBiase and Lamb, 2020) but is generally absent in burned sites that produce debris flows in Arizona (Raymond et al., 2020) and New Mexico (McGuire and Youberg, 2020). Following wildfire in the San Gabriel Mountains, dry ravel transports sediment stored in dams behind vegetation on steep hillslopes down into the channel network where it provides a relatively fine and cohesionless source of sediment for debris flows (Florsheim et al., 1991; Lamb et al., 2011; Palucis et al., 2021; DiBiase and Lamb, 2020). PFDFs in the Transverse Ranges are often associated with cool-season precipitation, especially short-duration (≤ 30 min) bursts of intense rainfall that accompany longer-duration atmospheric river events (Oakley et al., 2017). In contrast to sites where dry ravel plays a substantial role, McGuire and Youberg (2020) documented 24 debris flows following a fire in the Tularosa Mountains of western New Mexico where dry ravel was not observed and sediment was eroded primarily from cohesive soils and colluvium stored in unchannelized valley bottoms during short-duration, convective rainstorms associated with the North American Monsoon. Given the increases observed in the number and severity of fires in New Mexico (Singleton et al., 2019), efforts to quantify the characteristics of debris flow



triggering rainfall in this region and explore differences and similarities with other regions of the southwestern USA would provide valuable decision-support science.

100 Similarly, there are complex and site-specific relationships between soil burn severity and the vegetation, ground cover, and soil properties known to affect PFDF initiation processes. While soil water repellency has received substantial attention for its potential to increase runoff, sediment yield, and debris flow activity following fire (e.g., Scott and van Wyk, 1990; Wells, 1987), increases in runoff and debris flow activity also occur in areas burned at moderate to high severity despite increases in soil infiltration capacity relative to nearby unburned soils (Raymond et al., 2020). In other cases, a combination of fire-induced changes have been implicated in contributing to increased debris flow susceptibility in areas burned at moderate to high severity, including reductions in interception, hydraulic roughness, infiltration capacity, and soil cohesion (McGuire and Youberg, 2020; McGuire et al., 2021; Peduto et al., 2022). Although the fire-related impacts that are most important are site specific, identifying fire-related impacts that most commonly increase debris flow activity supports the production of more generalizable models to assess post-fire debris flow hazards. Pairing post-fire debris flow observations with measurements of fire-related impacts in areas burned at different severities could help identify the fire-related impacts that play the most important roles in promoting debris flow activity.

115 In addition to varying spatially with soil burn severity, the effects of fire on soil and vegetation change with time since fire, which in turn influences runoff and sediment transport processes, including debris flow potential (Ebel, 2020; Hoch et al., 2021; Thomas et al., 2021). The potential for PFDFs generated by runoff is greatest immediately following fire, yet effects of fire on soil hydraulic properties and vegetation may persist and continue to modify debris flow potential for years (Ebel and Martin, 2017; Hoch et al., 2021; Thomas et al., 2021). DeGraff et al. (2015) analysed a database of 75 PFDFs throughout the western USA to determine that 71% of PFDFs occurred within the first 6 months following fire and 85% within the 12 months. While the decrease in debris flow observations after more than 1 year of recovery is encouraging from a hazard perspective, it also means that there is a general paucity of data available for developing empirical models for PFDF likelihood throughout the recovery period. Monitoring efforts that extend beyond the first year following fire will lead to better constraints on changes in rainfall ID thresholds for PFDFs over time and will support the development of data-driven models for PFDF likelihood that extend through the window of disturbance following fire.

125 In this study, we take advantage of a natural experiment set up by the 2020 Tadpole Fire, which burned over steep terrain in western New Mexico, to investigate PFDF processes. The main objectives of this study were to (1) monitor a series of burned watersheds to assess spatial variations in debris flow activity and the temporal persistence of debris flow activity during the first three monsoon seasons following the fire, (2) quantify differences in soil hydraulic properties and ground cover over time in areas with different soil burn severity to help explain observed differences in the spatial and temporal distribution of debris flows, and (3) constrain the timing of debris flows within rainstorms to quantify rainfall thresholds for debris flow initiation



130 and examine rainfall characteristics of debris flow-producing storms. An overarching goal of this work is to provide data and
process insights that could improve situational awareness of PFDF hazards and data-driven models of debris flow likelihood
135 (Kern et al., 2017; Staley et al., 2017; Nikolopoulos et al., 2018) that can be used to assess PFDF hazards.

2 Study Area

The Tadpole Fire burned over 40 km² in the Gila National Forest in June 2020 before being contained in July 2020 (Figure 1).
135 Vegetation is dominated by ponderosa pine (*Pinus ponderosa*), and the area is underlain by tertiary-aged volcanic rocks
(Scholle, 2003). Rainfall at the site occurs primarily during the summer, as part of the North American Monsoon, as well as
during the winter months. Summer rainstorms during monsoon season are characterized by relatively short durations and high
intensities, whereas rainstorms during the winter months tend to have greater durations and lower peak intensities over short
(< 60 minutes) duration. Peak 15-minute rainfall intensities of 1-yr and 10-yr recurrence interval storms are 50 mm/h and 99
140 mm/h, respectively (Bonnin et al., 2011).

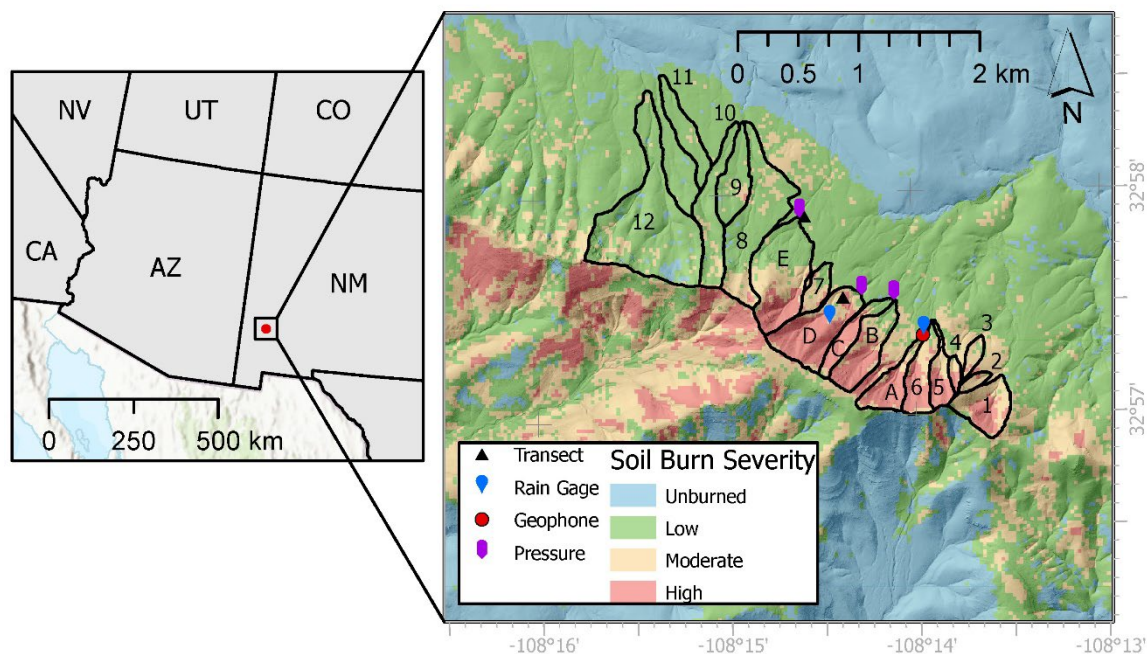


Figure 1: The 2020 Tadpole Fire burned in southwestern New Mexico, USA. Monitored watersheds are outlined in black. Intensively monitored watersheds are labelled from A-E from east to west and other monitored watersheds are labelled from 1-12 from east to west.



145 Bedrock-dominated channels drain portions of the steep, upper watersheds before transitioning to more moderately sloping valleys, which lacked incised channels or gullies and had limited bedrock exposure (Figure 2). Soil burn severity, which was assessed following the fire by the Burned Area Emergency Response (BAER) team, was spatially variable across the study area. The upper, steep slopes of watersheds in our monitoring area generally burned at higher severity relative to those at lower elevations. Soil burn severity classifications of low, moderate, and high are determined for different portions of the landscape
150 based on a combination of field assessments and satellite-derived products, specifically the differenced normalized burn ratio (dNBR) (Key and Benson, 2006). A map of dNBR was created using satellite images from before and after the fire (Miller and Thode, 2007). The dNBR thresholds for low, moderate, and high soil burn severity are then determined based on a field-

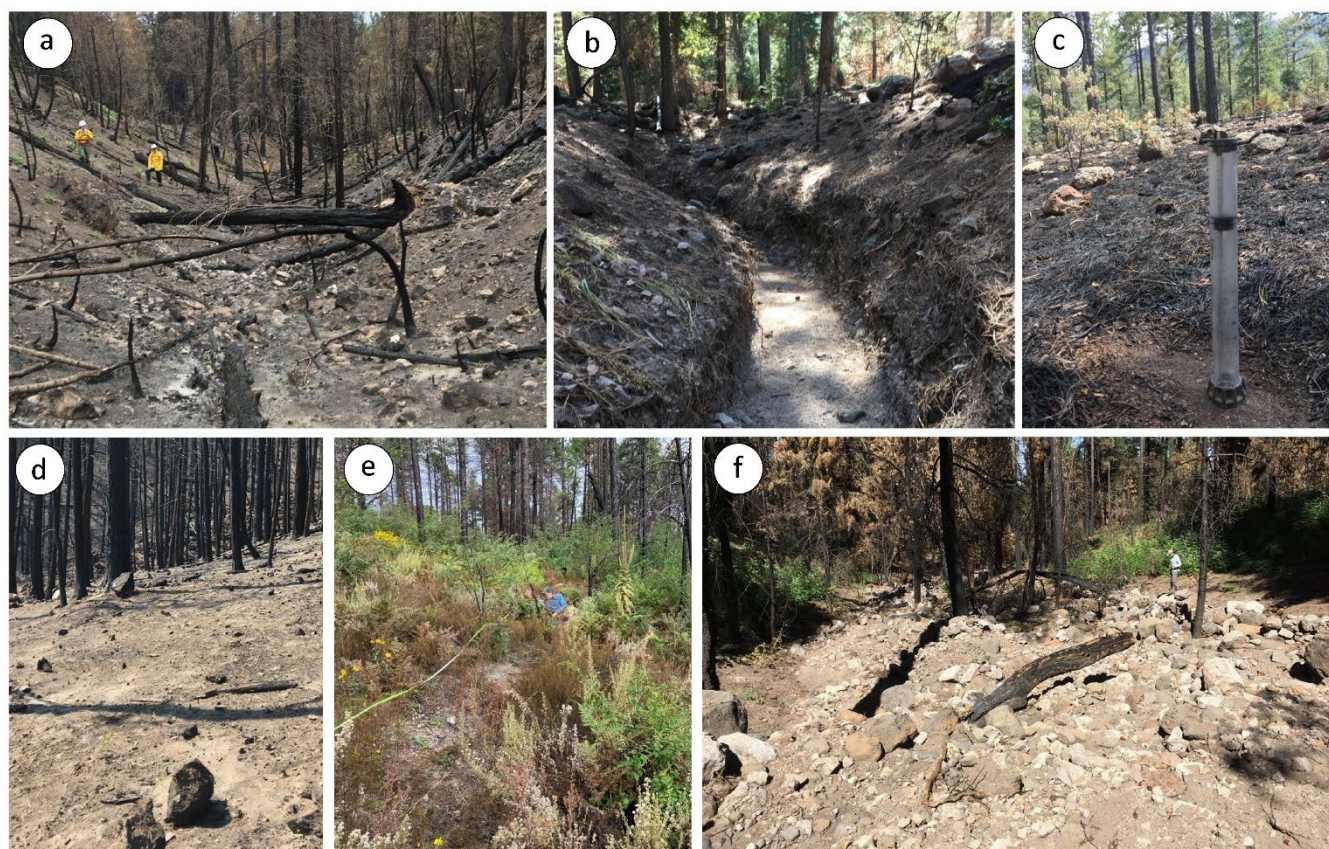


Figure 2: Examples of (a) the unchanneled valley bottoms that drained the lower portions of many watersheds prior to post-fire rainfall and a (b) gully incised by post-fire rainstorms during the 2020 monsoon season. (c) A minidisk tension infiltrometer set up for a measurement at the mineral soil surface in an area with low soil burn severity. Note abundant needle cast and green canopy on trees in the background. (d) Canopy and ground cover were negligible shortly following the fire in July 2020 at the location of the moderate/high severity vegetation transect. (e) Understory canopy and litter cover substantially limited the fraction of bare ground at the moderate/high severity transect by September 2022. (f) Example of a debris flow deposit immediately upstream of Forest Road 3131A.

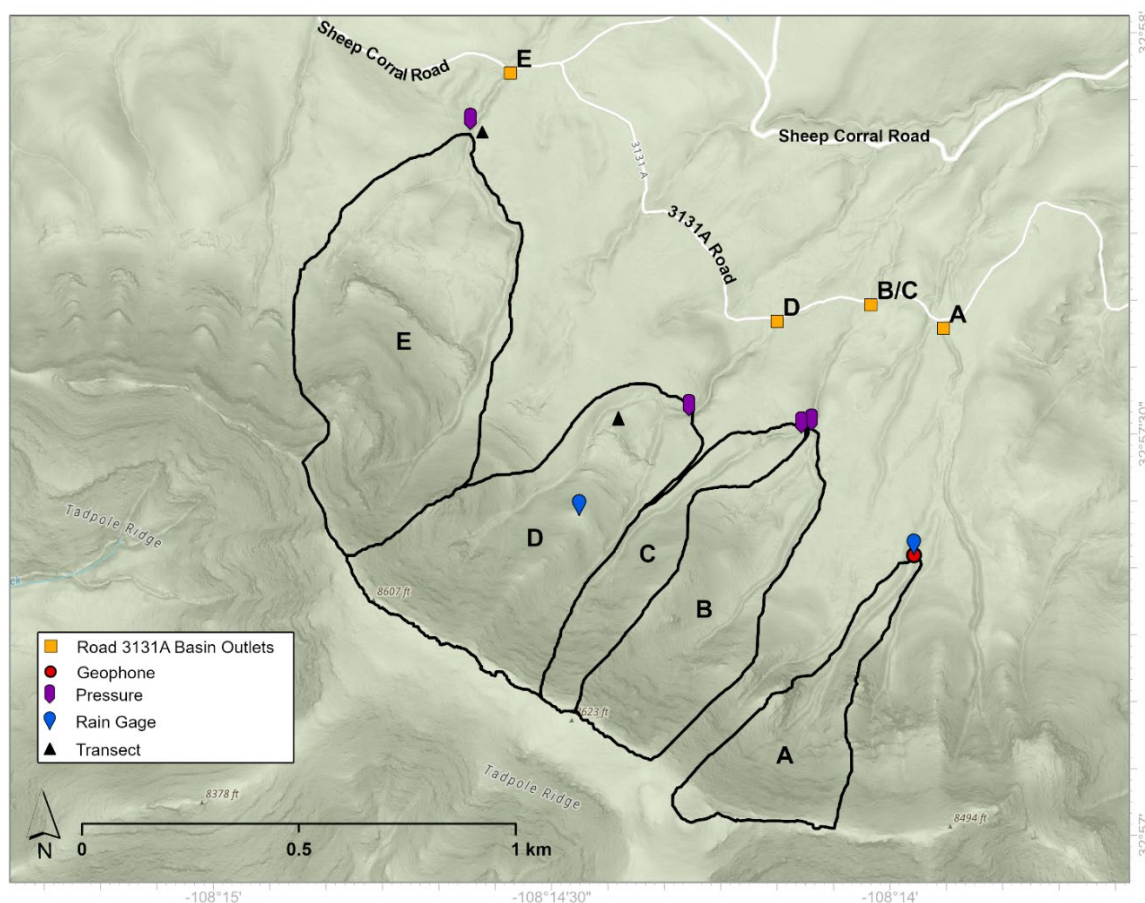
160 based assessment of the effects of the fire on the soil in different locations (Parsons et al., 2010). The classified soil burn severity map was then created based on these thresholds. In July 2020, less than a month following the fire, we observed that canopy and ground cover were negligible in areas burned at moderate and high soil burn severity whereas canopy and ground



cover, including a substantial amount of charred pine needles, were present to varying degrees in areas burned at low severity (Figure 2).

165 3 Methodology

Within one month, and prior to any measurable rainfall, following the start of the Tadpole Fire on 6 June 2020, we began monitoring debris flow activity and established sites within the burned area where we repeatedly made measurements to quantify soil hydraulic properties, ground cover, and understory canopy cover (Figure 1). The monitoring period for this study extended from June 2020 through October 2022. During the first post-fire monsoon season, we monitored debris flow activity
170 in seventeen watersheds, all of which drain to the northeast from Tadpole Ridge and have elevations that range from approximately 2300 m to 2600 m (Figure 1). However, after the first monsoon season ended in September 2020, subsequent



175 **Figure 3:** The five intensively monitored watersheds, referred to as watersheds A-E, drain to the northeast off Tadpole ridge towards the 3131A Road and Sheep Corral Road. During debris flow-producing storms, sediment often deposited where the channels intersect these roads (yellow squares).



180 flow monitoring efforts throughout the remaining 2+ year monitoring period focused on five intensively monitored watersheds (Figure 1). The four eastern-most of these five watersheds, referred to as watersheds A, B, C, and D, drain down towards the 3131A road, a dirt road that runs roughly perpendicular to the direction of flow (Figure 3). Flows exiting watershed E similarly drain towards Sheep Corral Road. Sheep Corral Road also intersects the channels that drain watersheds A-D roughly 500 m downstream of the 3131A road. These roads provided access to the study area and often promoted deposition of debris flow sediment.

3.1 Ground Cover and Infiltration Measurements

We monitored changes in ground cover and understory canopy cover along two hillslope transects using the line-point intercept method (Crocker and Tiver, 1948) to explore how temporal changes in ground cover affect debris flow activity (objectives 1 and 2). One transect was located in an area burned at moderate/high severity, while the other was located in an area burned at low severity (Figure 1). Both transects were 20 m in length, and we made measurements at 20 cm intervals to determine the presence of canopy, litter, soil, or rock. Here, canopy refers only to standing vegetation from the ground surface to eye level and therefore does not quantify canopy that remained on mature trees in the low burn severity area (Figure 2). We characterized all loose plant material (i.e., not connected to standing vegetation) on the soil surface as litter, including charred needles and woody debris. Any clasts at or embedded within the soil surface that had a diameter greater than 5 mm were classified as rocks. The percentage of total ground cover was determined based on the number of first hits that were classified as either canopy or litter while bare ground consisted of all measurements where the first hit was soil or rock. We conducted ground cover surveys on 6 July 2020, 11 May 2021, and 30 September 2022.

195 Soil hydraulic properties vary spatially, due to variations in soil burn severity and material properties, and temporally as the landscape recovers (Moody et al., 2016; Ebel et al., 2022). Therefore, in support of objective 2, we periodically conducted in-situ infiltration measurements over 2+ years using minidisk tension infiltrometers in areas burned at moderate/high severity and low severity as well as a nearby unburned area (Figure 2c). We made measurements shortly following fire in areas burned at moderate/high severity (July 2020) and low severity (August 2020) and assessed changes over time by also making measurements in both severity classes in May 2021, May 2022, and September 2022. Measurement locations were determined opportunistically and at varied locations within the study area in 2020 and were then co-located with the vegetation transects in subsequent visits. Measurements made alongside the vegetation transects were spaced at least 1 m apart. The number of measurements for a given group varied from a minimum of 6 to a maximum of 20. All measurements were made at the surface of mineral soil, after brushing aside any ash or litter, with 1 cm of suction.

205 Measurements resulted in a record of cumulative water volume infiltrated, I , as a function of time, t . We used this time series, following the methodology of Zhang (1997), to estimate field-saturated hydraulic conductivity, K_{fs} , and sorptivity, S . In particular, Zhang (1997) demonstrated that



210

$$I = C_1\sqrt{t} + C_2t \quad (1)$$

where $C_1 = A_1S$ and $C_2 = A_2K_{fs}$ and $A_1 = 1.21$ and $A_2 = 5.72$ are empirical coefficients that depend on soil texture. The values for A_1 and A_2 used here are consistent with the soil texture at our site, which is classified as a loam. Therefore, K_{fs} and S can be estimated by fitting a curve to equation 1. In addition, we used estimates of K_{fs} and S to determine the wetting front potential, h_f , according to (Ebel and Moody, 2017)

215

$$h_f = \frac{S^2}{2K_{fs}(\theta_s - \theta_r)} \quad (2)$$

The wetting front potential is a parameter in the Green-Ampt infiltration model, which is commonly used in post-fire hydrologic models (Ebel, 2020; McGuire et al., 2016; Rengers et al., 2016, 2019). In the above equation, $\theta_s = 0.43$ denotes the soil moisture at saturation for a loam soil and we let the residual soil water content, $\theta_r = 0.078$, serve as an approximation for the initial soil moisture (Carsel and Parrish, 1988).

220

Vandervaere (2000) suggested three different curve-fitting techniques to estimate K_{fs} and S , all three of which we employ here. The first technique, the cumulative infiltration (CI) method, relies on fitting a quadratic function to

225

$$Y = C_1X + C_2X^2 \quad (3)$$

where $Y = I$ and $X = \sqrt{t}$. The cumulative linearization (CL) method is accomplished by dividing equation 2 by \sqrt{t} and fitting a line to the resulting relationship,

230

$$Y = C_1 + C_2X \quad (4)$$

where $Y = I/\sqrt{t}$ and $X = \sqrt{t}$. Lastly, the differentiated linearization (DL) method requires fitting a line to

$$Y = C_1 + C_2X \quad (5)$$

where $Y = dI/d\sqrt{t}$ and $X = \sqrt{t}$. We found, in agreement with Vandervaere (2000), that the DL and CL methods help identify measurements where infiltration does not meet the assumptions of the Zhang (1997) model. For example, in some cases, we observed nonlinear or piecewise linear trends when plotting equations 3 and 4, in which case fitting a line to these data would

235



result in erroneous estimates for K_{fs} and S . This could result from a multilayer infiltration system where there is a thin water repellent layer near the surface and a more wettable layer below. In these cases, we did not use the measurement to estimate K_{fs} and S . Otherwise, we took the average of the three K_{fs} values and the three S values resulting from the three curve-fitting techniques to arrive at a single estimate for K_{fs} and S for each measurement.

In the first summer following the fire, we additionally assessed soil water repellency at the surface of mineral soil and 2 cm below the surface using the water drop penetration time (WDPT) test. We conducted tests at eight different locations, six in areas burned at moderate or high severity and two burned at low severity. Three water drops were placed on the soil surface in each of the eight locations, roughly 10-20 cm apart, after removing any ash or litter. We recorded the time for each drop to be absorbed and then classified water repellency into one of four classes. Water drop penetration times of < 5, 5-60, and 60-180, and 180+ seconds were associated with no, slight, moderate, and extreme water repellency, respectively (Robichaud and Hungerford, 2000).

3.2 Modelled changes in runoff

We used a point-scale infiltration model to quantify how measured temporal changes in soil hydraulic properties, namely K_{fs} , S , and h_f , translated into temporal changes in runoff potential, a key variable for assessing PFDF susceptibility. Watershed responses to rainfall are affected in different ways by changes in K_{fs} , S , and h_f . Analysing impacts of fire on K_{fs} , S , and h_f in isolation may therefore lead to incomplete conclusions about the potential for runoff, a necessary condition for the initiation of runoff-generated debris flows, since fire-driven changes in K_{fs} may be entirely or partially offset by changes in h_f , or vice versa. Here, we use the Green-Ampt infiltration model to quantify the combined effects of K_{fs} and h_f on runoff generation (Green and Ampt, 1911). Specifically, infiltration capacity, I_c , is computed as

$$I_c = \frac{K_s(Z_f + h_f + h)}{Z_f}, \quad (6)$$

where K_s denotes the saturated hydraulic conductivity, $Z_f = V/(\theta_s - \theta_i)$ denotes the depth of the wetting front, V is the total infiltrated depth, $\theta_i=0.078$ is the initial soil moisture content, and h is the depth of overland flow. In the Green-Ampt model, the wetting front potential and saturated hydraulic conductivity, which we estimate using K_{fs} , control the capillarity and gravity contributions to infiltration, respectively. Given an input rainfall intensity, we used this infiltration model to assess changes in runoff ratio and peak runoff rate at the point scale (i.e., runoff is not routed over the landscape) over time in soils burned at moderate/high severity and at low severity. The runoff ratio for a rainstorm is defined as the ratio of the total runoff depth to the total rainfall depth. We compared simulated runoff ratios and peak runoff rates from burned soils with those computed for unburned soil conditions.



270 Since rainfall intensity averaged over 15-minute time intervals has proven to be a good predictor for PFDF initiation in the southwestern USA (Staley et al., 2017, 2013; Raymond et al., 2020), we computed runoff ratios in response to design rainstorms with 15-minute durations. We considered six different rainstorms characterized by average rainfall intensities that are equal to the 1-, 2-, 5-, 10-, 25-, 50-, and 100-year recurrence interval rainstorms (Bonnin et al., 2011). Since there are distributions of K_{fs} and h_f for a given time since fire and burn severity class, we used the geometric mean of K_{fs} as an estimate for K_s (Liu et al., 2023). Similarly, we determined a representative parameter value of h_f in simulations based on the geometric mean of the h_f distribution derived from the mini disk measurements. The main objective of simulations is to assess the combined effects of changes in K_{fs} and h_f on runoff generation in response to different magnitudes of rainfall intensity.

280 We numerically approximated changes in infiltration and runoff rates over time, t , during a design rainstorm based on the difference between the rainfall rate, R , and the infiltration capacity determined by equation 6. More specifically, we separated the rainstorm into a series of time steps of duration $\Delta t = 1$ second. Letting n denote the value of a quantity at a particular time step and assuming a negligible depth of overland flow, infiltration capacity can be computed as

$$I_c^n = \min\left(\frac{K_{fs}(Z_f^n + h_f)}{Z_f^n}, R^n\right). \quad (7)$$

The runoff rate, q , at time step n can be taken as $q^n = \max(R^n - I_c^n, 0)$. Then, the total infiltrated depth and depth of the wetting front can be updated according to

285

$$V^{n+1} = V^n + \Delta t I_c^n \quad (8)$$

and

$$Z_f^{n+1} = \frac{V^{n+1}}{\theta_s - \theta_i} \quad (9)$$

We set $\theta_i = 0.078$ in all simulations. We summarized the simulated response during each storm by computing the runoff ratio and peak runoff rate.

3.3 Rainfall and Flow Monitoring

290 We installed equipment to quantify flow timing, flow type (i.e., debris flow, flood), and rainfall intensity to determine the rainfall characteristics associated with debris flow initiation in five intensively monitored watersheds during the first three monsoon seasons following the fire (objectives 1 and 3) (Figure 1; Figure 3). We also made observations to determine the presence/absence of debris flow activity in 12 additional watersheds during the first post-fire monsoon season but did not



attempt to constrain flow timing in these instances (Figure 1). Two tipping bucket rain gauges recorded rainfall accumulation
295 over time in increments of 0.2 mm (Figure 1). We installed non-vented pressure transducers near the outlets of watersheds B,
C, D, and E, which provided information about flow type and timing (Figure 1; Figure 3). We installed the pressure transducers
by recessing them into a hole drilled into the bedrock channel. Two geophones (single-component, Geospace GS 11) monitored
flow in watershed A by recording at a rate of 50 Hz (Figure 1). Interpretation of geophone and pressure transducer data,
described below, was aided by photos from time lapse cameras installed near several watershed outlets (Figure 1). The cameras
300 captured photos on time intervals ranging from 3-60 minutes depending on battery life, memory capacity, and expected timing
of subsequent visits to service equipment. The equipment was installed in early July 2020 prior to any post-fire rainstorms.

The two geophones in watershed A were installed outside of the channel, roughly 15 meters from the channel thalweg, and
were separated by approximately 18 meters (Rengers et al., 2023). Geophone data were filtered between 5 and 20 Hz, and the
305 instrument response was removed, converting the signal to ground velocity. Data are displayed as signal power and short-time
Fourier transforms calculated using a 5-second moving window. Seismic data help determine flow type, especially when paired
with cameras and frequent field observations, since debris flows produce intense ground vibrations relative to floods (McGuire
et al., 2018; Kean et al., 2015). Debris flow activity is also generally characterized by an abrupt increase in signal power, over
a wide range of frequencies, that tapers gradually (Porter et al., 2021). We used these characteristic features of the signal to
310 estimate, to the nearest minute, the time that debris flows passed by the geophones.

The non-vented pressure transducers recorded variations in pressure on 1-minute intervals. Pressure can change due to
variations in atmospheric pressure, depth of flow in the channel, and changes in sediment thickness on top of the sensor due
to deposition or erosion. Data from these sensors are therefore not ideal for obtaining absolute estimates of flow depth, but
315 they provide an effective and low-cost method to determine flow timing and flow type during rainstorms, especially when
paired with post-event field observations (Kean et al., 2012). A rapid increase and subsequent decrease in pressure over a short
time is typically observed during the passage of a debris flow whereas the temporal variations in pressure associated with a
flood are characterized by a more gradual increase and then decrease in pressure. We therefore used the time series of pressure
to identify the time at which debris flows exited the monitored watersheds. Given the relatively small size of the watersheds
320 (< 1 km²) and location of the pressure transducers within hundreds of meters of the ridgeline, we estimate that the time
difference between debris flow initiation and the debris flow passing by a pressure transducer or geophone is limited to several
minutes. A debris flow could travel a distance of 500 m from an initiation location to a pressure transducer in less than two
minutes assuming an average velocity of 5 m/s. In addition to utilizing the pressure transducer and geophone data to assess
flow type and timing, we also field-verified the occurrence of a debris flows by making post-event observations of deposit
325 morphology within and downstream of the monitored watersheds, as described in more detail below.



3.4 Rainfall characteristics

3.4.1 Intensity, recurrence, and temporal variability

To assess rainfall characteristics, we computed rainfall intensities over durations ranging from 5 minutes to 60 minutes. More specifically, we defined

330

$$I_D(t) = \frac{R(t) - R(t - D)}{D} \quad (10)$$

335

as the average rainfall intensity over D minutes. Although I_D will vary throughout a rainstorm, it has proven useful to summarize rainfall characteristics using the peak value of I_D for the development of rainfall intensity-duration thresholds for debris flow initiation. Past studies have demonstrated that I_{15} is a particularly useful metric for assessing debris flow likelihood during a post-fire rainstorm (Staley et al., 2013), possibly because the debris flows are frequently generated by runoff and runoff is correlated well with rainfall averaged over a 15-minute duration in small, steep, recently burned watersheds (Kean et al., 2011; Raymond et al., 2020). In cases where we could constrain the timing of debris flows within rainstorms using the pressure time series and geophone data, we estimated the rainfall intensity responsible for triggering the debris flow (i.e., triggering intensity) by finding the peak value of I_D within a 15-minute time window prior to the detection of the debris flow at the pressure sensor for values of D from 5, 10, 15, 30, and 60 minutes (e.g., McGuire and Youberg, 2020).

340

The steep, upper slopes of all 17 monitored watersheds, which is where debris flows are most likely to initiate, were all located within approximately 2 km of both rain gages. We used the rain gage closest to each watershed to determine rainfall characteristics associated with events (i.e., a debris flow) at that watershed. During the second and third monsoon seasons, in 2021 and 2022, respectively, the rain gage in watershed D was knocked down, likely by an animal, at an unknown time. Therefore, we only utilized data from the rain gage in watershed A during those two time periods. Rain gages were only maintained from late spring to early fall to capture data during the monsoon season when debris flows were likely to initiate and when precipitation occurred entirely as rainfall.

345

We computed the recurrence interval of all rainfall intensities that produced debris flows, focusing on average intensity over a 15-minute duration given its particular relevance for PFDFs in this region (Kean et al., 2011; Staley et al., 2013; Raymond et al., 2020). Following the methodology from Staley et al. (2020), we determined recurrence intervals for observed rainfall intensities by fitting a curve to the 1-, 2-, 5-, 10-, 25-, 50-, and 100-year recurrence interval intensities as determined by NOAA Atlas 14 (Bonnin et al., 2011). To further analyse rainfall at our study site, we examined the temporal distribution of rainfall within storms using the standardized rainfall profile (SRP) approach described by Huff et al. (1967) and recently applied to the study of PFDFs by Esposito et al. (2023). The SRPs represent the cumulative fraction of storm rainfall as a function of the

355



fraction of storm duration, allowing for a rapid visual assessment of the temporal distribution of rainfall within a storm (Figure S1). Convective storms tend to be characterized by SRPs that lie above the 1 to 1 line whereas frontal storms often have SRPs that lie below the 1 to 1 line (Esposito et al., 2023). We further classified rainstorms based on the quartile of storm duration that contains the highest cumulative rainfall total. Storms where more rainfall occurred during the first quartile of the storm duration were classified as Q1 storms while those with more rainfall during the 2nd, 3rd, or 4th quartile of the storm duration were classified as Q2, Q3, and Q4 storms, respectively (Huff, 1967).

3.4.1 Intensity-duration threshold

Rainfall intensity-duration (ID) thresholds, which define a curve in intensity-duration space above which debris flow initiation is likely, are a practical tool for post-fire debris flow warning and hazard assessment (Cannon et al., 2008; Staley et al., 2013; Esposito et al., 2023). They are also a convenient way to summarize the rainfall characteristics responsible for triggering debris flows so they can be compared with findings from other regions. We followed the methodology of Staley et al. (2013) to objectively define rainfall intensity thresholds for durations of 5, 10, 15, 30, and 60 minutes (objective 3).

For a given duration, D , we use records of rainfall intensity and watershed response to test the performance of intensity thresholds that vary from 1 to 200 mm/h on 0.1 mm/h intervals. We use the threat score, TS , to assess the performance of each potential intensity threshold. The intensity threshold for a given duration is defined based on which of the tested intensities results in the highest TS . The threat score is defined as

$$TS = \frac{TP}{TP + FN + FP} \quad (11)$$

where TP, FN, and FP denote the number of true positives, false negatives, and false positives. A true positive occurs when the rainfall intensity exceeds the threshold and a debris flow is observed. A false negative occurs when the rainfall intensity lies below the threshold, but a debris flow is observed. A false positive occurs when rainfall intensity is above the threshold and no debris flow is observed. Potential thresholds are therefore penalized when they incorrectly classify an event (i.e., FN or FP).

3.5 Debris Flow Surveys

During the first post-fire monsoon season, we conducted field surveys at all five of the intensively monitored watersheds on 29 July 2020, 14 August 2020, 31 August 2020, and 17 October 2020 to determine which watersheds produced debris flows during the first monsoon season following the fire. Also on 17 October 2020, we visited 12 nearby watersheds and used presence and absence of debris flow deposits to assess whether there had been debris flows at any point since the fire. In subsequent years, we made pre- and post-monsoon season visits to conduct field surveys but limited our observations to the



390 five watersheds initially chosen for intensive monitoring. Characteristics associated with debris flow deposits include lateral levees and poorly sorted, matrix-supported deposits that lack imbrication (Figure 2) (Costa, 1988; Pierson, 2005). We used these characteristic debris flow depositional patterns as an indicator of debris flow activity in a watershed. If no debris flow deposits were found within a watershed, the drainage was classified as having a flood response or no response during all rainstorms that occurred within the monitoring period. In cases where we determined that a debris flow occurred but we could not constrain the timing of debris flow, we assigned the triggering intensity to be equal to the peak rainfall intensity observed in any storm prior to the debris flow survey.

395 We quantified the grain size distribution of six debris flow deposits during the first monsoon season following the fire by collecting samples in 1/2-gallon bags. These samples were air dried and sieved to quantify the particle size distribution of sediment greater than 2 mm. Percentages of sand, silt, and clay were quantified with the hydrometer method. We did not include any sediment greater than gravel-sized in these samples, but we did perform pebble counts (Bunte and Abt, 2001) at two deposits to estimate the size distribution of the coarser sediment in the flow. We completed pebble counts within watershed
400 A (latitude: 32.96085, longitude: -108.23568) and watershed D (latitude: 32.961053, longitude: -108.236013) by extending a measuring tape in a transect across a debris flow deposit and measuring the B-axis of clasts on a 25 cm interval. If the clast was too small to be measured, it was recorded as fine sediment (<2 mm). The sample spacing of 25 cm was chosen based on the size of boulders in the deposit to minimize the likelihood of encountering the same clast twice. No clasts were counted twice.

405 3.5 Terrain Analysis

We analysed the morphologic properties and burn severity characteristics of the monitored watersheds to help interpret any observed spatial variations in debris flow susceptibility. Watershed outlets for intensively monitored watersheds were defined based on the locations of flow monitoring equipment (i.e., geophones, pressure transducers), and watershed outlets for the remaining watersheds were defined based on the farthest downstream point where detailed field observations were made to
410 assess flow type. We focused on quantifying watershed properties related to slope, soil burn severity, and soil erodibility since prior studies have shown these to be particularly relevant for assessing debris flow likelihood at the watershed scale (Cannon et al., 2010; Staley et al., 2017). We consider mean watershed slope, and the fraction of area burned moderate or high severity, the soil KF factor (*KF*), the fraction of area that is greater than 23 degrees and burned at moderate or high soil burn severity (*MH23*), and average *dNBR*. The first two factors related to slope and burn severity have general relevance to debris flow
415 initiation by runoff since steeper, more severely burned watersheds are more likely to experience greater increases in runoff and sediment transport. The last three factors, along with the peak 15-minute rainfall accumulation, R_{15} , are inputs for the M1 debris flow likelihood model (Staley et al., 2017) (Table S3). The M1 model is a logistic regression model, which was trained using a debris flow database from southern California and tested using data throughout the western USA (Staley et al., 2017). The model yields watershed-scale predictions for debris flow likelihood, p , according to



$$p = \frac{e^X}{1 + e^X} \quad (12)$$

420

where

$$X = 0.41R_{15}MH23 + 0.67R_{15} \frac{dNBR}{1000} + 0.7R_{15}KF \quad (13)$$

In addition, the model equations can be rearranged to solve for the rainfall intensity required over a 15-minute time period in order for the likelihood of a debris flow to be 0.5 (Staley et al., 2017). Following Staley et al. (2017), we used the M1 model to compute a 15-minute rainfall intensity-duration (ID) threshold, I_{15}^{M1} , for each watershed based on rainfall needed to achieve $p = 0.5$. We compared these thresholds with observed values of I_{15} that triggered debris flows in each watershed in our study area. We further compared spatial variations in I_{15}^{M1} with observed variations in debris flow activity. One goal of these comparisons is to help assess the extent to which watershed morphologic factors that control debris flow initiation processes are similar or different among our site and the sites in southern California where the M1 model was trained.

430 4 Results

4.1 Temporal changes in ground cover, infiltration capacity, and runoff

A substantial amount of bare ground was exposed in areas burned at moderate/high soil burn severity relative to areas burned at low severity in the immediate aftermath of the fire. The vegetation transect surveys on 6 July 2020 indicated 51% bare ground at the moderate/high severity transect compared to 9% bare ground at the low severity transect (Table 1). The fraction

435

Soil Burn Severity	Measurement Date	Months since fire	Understory Canopy (%)	Litter (%)	Total Ground Cover (%)	Bare Ground (%)
Low	6 July 2020	0	2	89	91	9
Low	11 May 2021	10	1	94	94	6
Low	30 Sep 2022	26	0	91	91	9
Mod/High	6 July 2020	0	8	41	49	51
Mod/High	11 May 2021	10	0	81	81	19
Mod/High	30 Sep 2022	26	79	69	89	11

Table 1: Estimates of understory canopy cover and ground cover from 101 measurements along 20 m transects. Months since fire is determined from containment in July 2020.

440 of bare ground exposed at the moderate/high severity transect decreased markedly by the second survey, conducted on 11 May 2021. By this time, roughly 10 months later, a substantial increase in litter cover reduced the percentage of bare ground to

19%. By September 2022, canopy and litter cover increases further reduced the percentage of bare ground to only 11% at the moderate/high severity transect. There was little change over this same time at the low severity transect, with the percentage of bare ground varying between 6% and 9%.

445

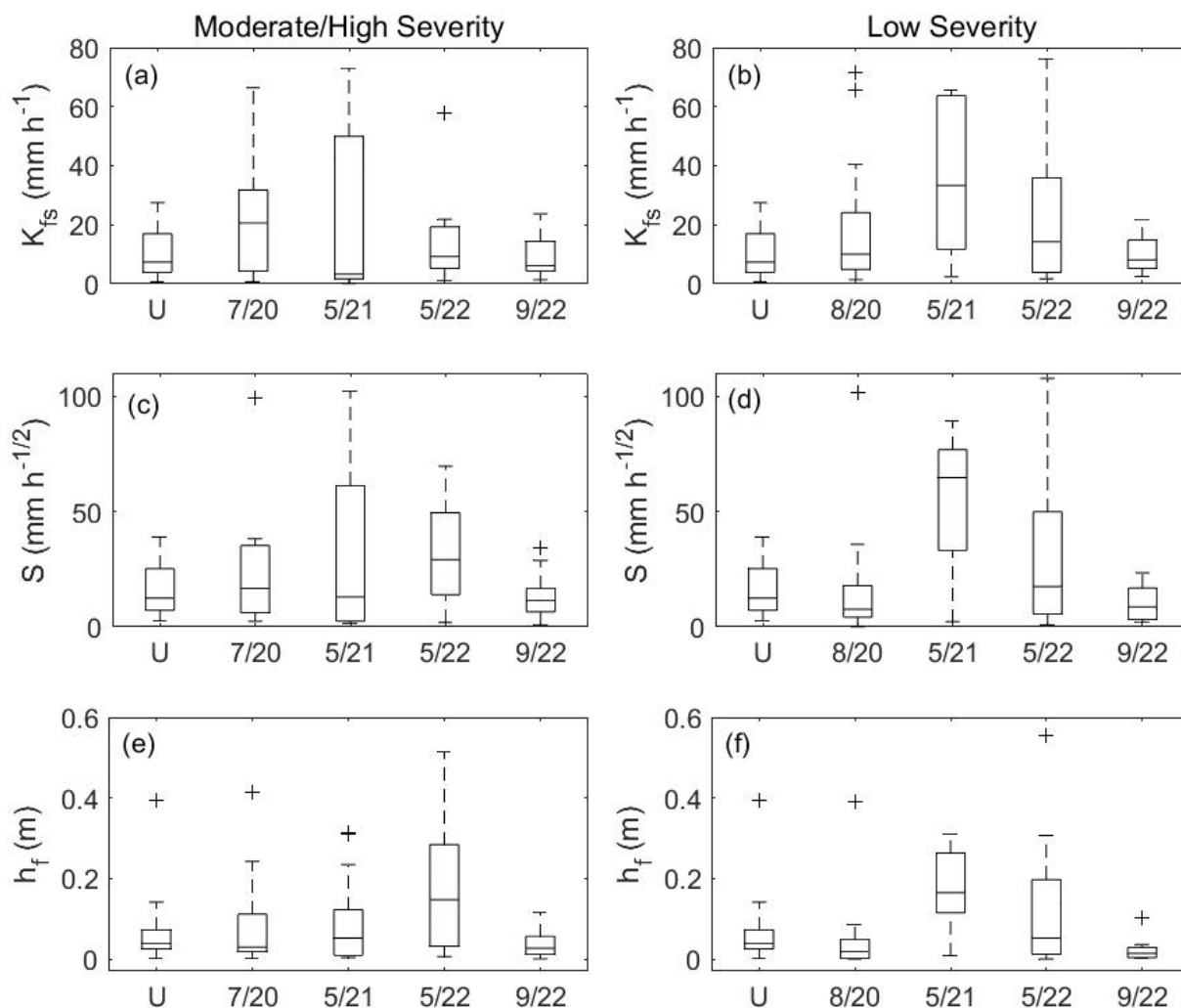


Figure 4: Minidisk infiltrometer measurements provide estimates of soil hydraulic properties and their temporal evolution following the fire in July 2020 relative to nearby unburned soils (U). Results indicate non-monotonic trends over time in (a, b) field-saturated hydraulic conductivity, K_{fs} [mm/h], (c, d) sorptivity, S [mm/h^{1/2}], and (e, f) wetting front potential, h_f [m]. Lines inside each box represent the median while box edges mark the first and third quartiles.

450

The median field-saturated hydraulic conductivity, K_{fs} , was slightly greater in areas burned at moderate/high severity in the first few months following the fire relative the unburned area, though a Kruskal-Wallis test indicated no significant differences in the median of the distributions ($p=0.27$) (Figure 4). The geometric means of K_{fs} in moderate/high severity, low severity, and unburned soils were 12 mm/h, 11 mm/h, and 7 mm/h, respectively (Table 2). A Kruskal-Wallis test also indicated no significant



455 differences in the median of the distributions of sorptivity in areas burned at different severities in the first few months following the fire ($p=0.24$). The geometric mean of S varied from $16 \text{ mm h}^{-1/2}$ in soils burned at moderate/high severity to $6 \text{ mm h}^{-1/2}$ and $12 \text{ mm h}^{-1/2}$ in soils burned at low severity and unburned, respectively (Table 2). Soil water repellency, which was greater at the surface than at 2 cm depth, also did not differ substantially from areas burned at moderate/high severity to areas burned at low severity in the first month following the fire (Figure S2). At the soil surface, approximately 55% of WDPTs indicated moderate or extreme water repellency in areas burned at moderate/high severity compared with 33% of measurements in low severity areas. We did not track temporal changes in soil water repellency but estimates of soil hydraulic properties show non-monotonic changes over time in the median and geometric mean of K_{fs} , S , and h_f (Figure 4, Table 2).

Soil Burn Severity	Measurement Date	Months since fire	Geo. mean K_{fs} [mm/h]	Geo. mean S [mm/h ^{1/2}]	Geo. mean h_f [m]	Number of measurements
Unburned	Oct 2020	-	6.8	12.31	0.035	16
Low	Aug 2020*	1	11.2	6.39	0.006	18
Low	May 2021	10	22.4	36.01	0.113	6
Low	May 2022	22	13	15.06	0.032	15
Low	Sep 2022	26	8.1	7.11	0.01	9
Mod/High	July 2020	0	11.5	15.95	0.037	13
Mod/High	May 2021	10	6.9	12.4	0.036	13
Mod/High	May 2022	22	9.6	22.62	0.09	16
Mod/High	Sep 2022	26	6.9	9.17	0.02	20

465 **Table 2:** Summary of soil hydraulic parameters estimated from minidisk tension infiltrometer measurements. We use the geometric mean (geo. mean) as a representative value for the distribution in numerical modelling. * Six measurements are also included from July 2020.

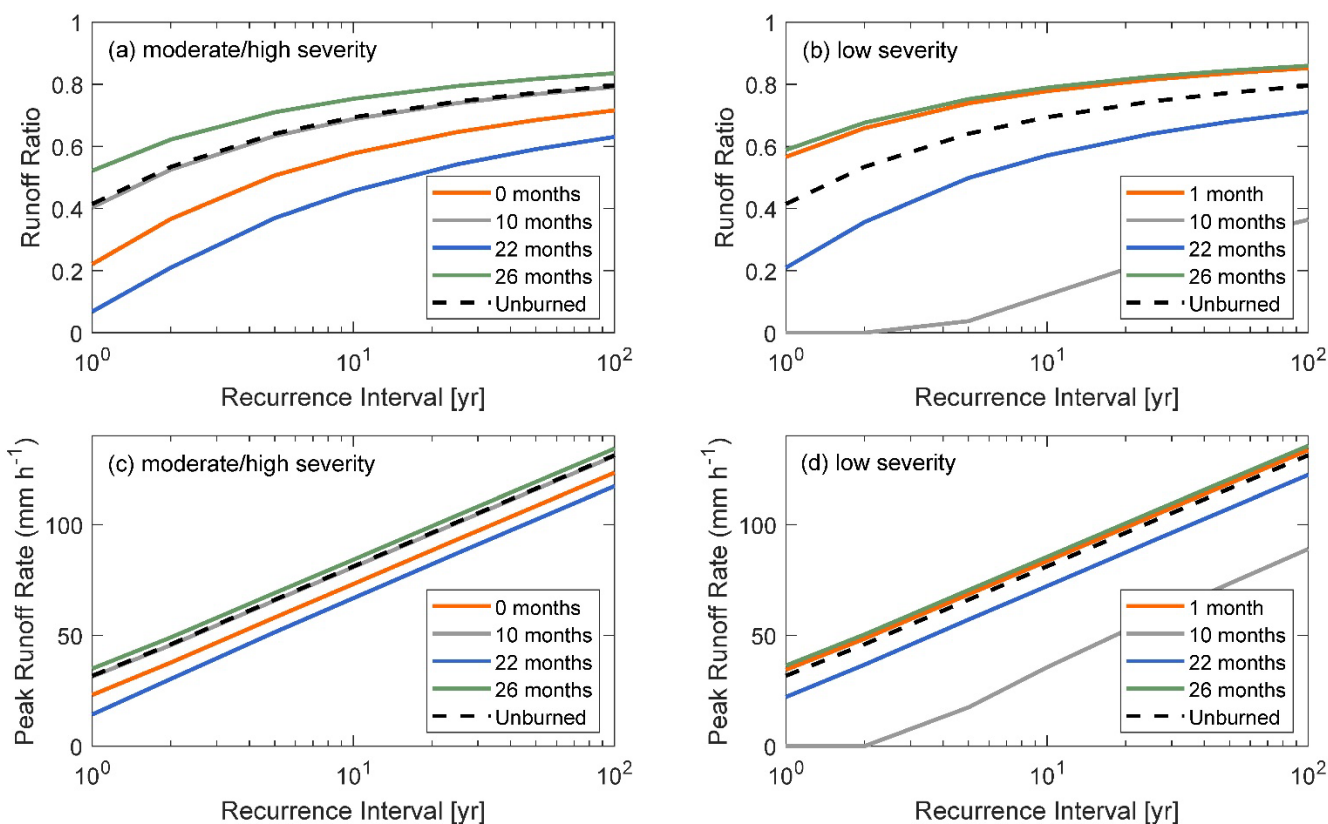
The point-scale rainfall-runoff model constrained by the minidisk measurements indicates that runoff ratios in areas burned at moderate/high severity were lower or similar to those simulated under unburned soil conditions after 0, 10, and 26 months of recovery. Runoff ratios increased slightly relative to unburned soil conditions after 20 months of recovery (Figure 5). Runoff ratios on soils burned at low severity were greater than unburned conditions after 1 and 26 months of recovery and lower than unburned conditions after 10 and 20 months of recovery. Peak runoff rates over time in areas of moderate/high and low burn severity followed similar patterns in terms of their values relative to those determined for unburned soil (Figure 5).

4.2 Spatial and temporal distribution of debris flow activity

475 We observed 16 debris flows during the first monsoon season following the fire, with the last debris flows occurring in early September 2020 (Table 3). There were no other debris flows during the remainder of the monitoring period, which extended through September 2022. Four of the five intensively monitored watersheds produced two or more debris flows, with watershed B being the exception. Watershed E was the only intensively monitored watershed to produce three debris flows, two of which



initiated during the same rainstorm. Six of the twelve additional watersheds that we surveyed at the end of the 2020 monsoon season produced debris flows following the fire, but we were unable to determine whether these watersheds produced multiple debris flows. We did not observe any evidence of dry ravel or mass failure (e.g. shallow landslides) on hillslopes. Following the debris flow-producing rainstorms in July and September, we observed rilling on hillslopes and gully erosion in areas of flow concentration (Figure 2b). Lateral levees and debris flow deposits downstream of areas of abundant channel and valley incision indicate debris flow initiation was facilitated by runoff and sediment transport processes rather than mobilization from shallow landslides on hillslopes.



485

Figure 5: Modelled runoff ratios for soils burned at (a) moderate/high severity and (b) low severity as well as modelled peak runoff rates for soils burned at (c) moderate/high severity and (d) low severity. Results for unburned conditions are shown for comparison. Design rainstorms are 15 minutes in duration with constant rainfall intensities associated with I_{15} recurrence intervals (RI) of 1, 2, 5, 10, 25, 50, and 100 years. In both moderate/high and low severity areas, runoff ratios and peak runoff rates oscillate back and forth, being higher or lower relative to unburned soils.

490

Debris flow-producing storms occurred on 18 July 2020, 21 July 2020, 24 July 2020, and 9 September 2020. The debris flows that initiated during the July rainstorms, which were less intense than the rainstorm on 9 September 2020, left terminal deposits on Forest Road 3131A and transitioned to water-dominated flood flows below the road. The debris flows triggered during the September rainstorm were characterized by longer runout distances and left additional deposits between the 3131A road and Sheep Corral Canyon Road (Figure 3). The fine fraction (< 2 mm) of debris flow sediment contained a higher concentration

495



of sand (58-82%) compared with two hillslope samples from 0-5 cm (43%) and similar amounts of clay, roughly 5-15% compared with an average of 12% on the hillslopes (Figure 6; Table S1). Sieve analyses of sediment samples from debris flow deposits yielded estimates of D_{50} that ranged from < 2 mm to 20 mm with a median of approximately 6 mm. The coarse fraction of debris flow deposit sediment, as quantified using pebble counts at watershed A and watershed D, had a D_{50} of 112 mm and 147 mm, respectively, and D_{90} of 259 mm and 335 mm, respectively (Figure 6).

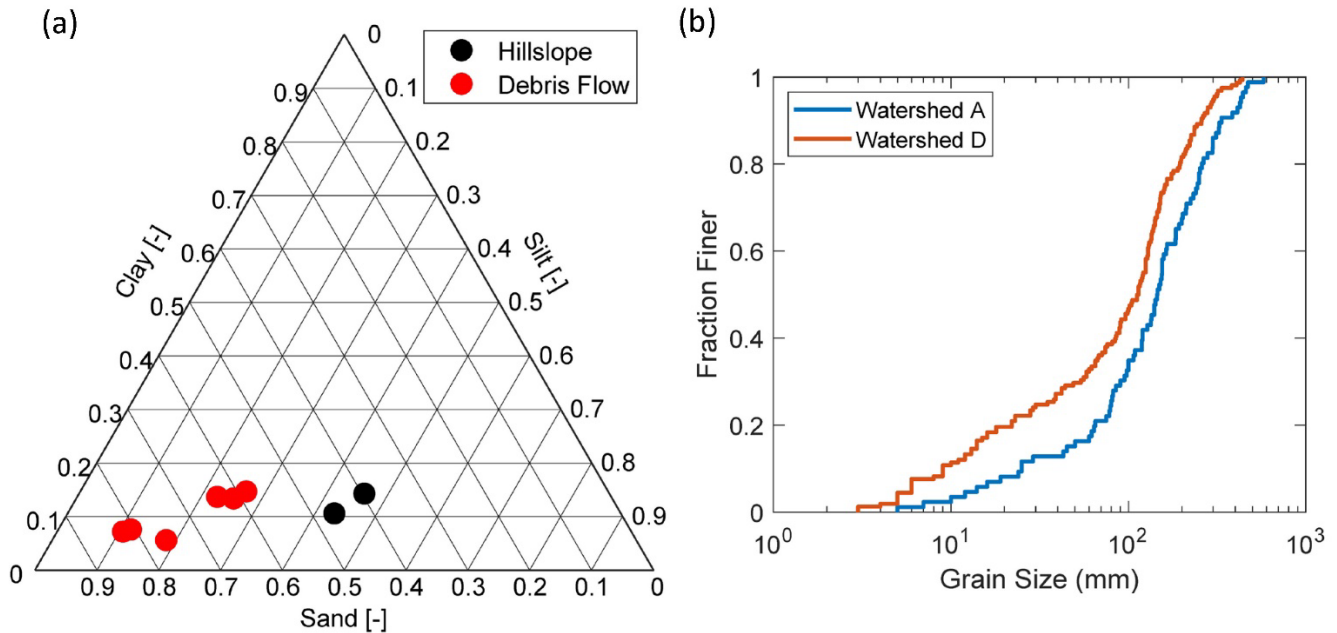
Watershed ID	Area [km ²]	Relief [m]	Mean Slope [deg]	Low SBS [%]	Mod. SBS [%]	High SBS [%]	I_{15}^{M1} [mm/h]	I_{15} [mm/h]	RI [yr]
1	0.15	238	29	7	54	39	16	86	5.4
2	0.02	190	28	3	84	13	16	86	5.4
3	0.03	205	22	13	79	8	26	-	-
4	0.02	171	31	4	48	48	16	86	5.4
5	0.08	274	31	3	33	64	14	86	5.4
6	0.13	270	26	7	38	55	16	86	5.4
A	0.12	292	29	2	28	69	15	33*, 76*	0.5, 3.4
B	0.18	314	26	15	30	55	17	53*	1.2
C	0.09	313	25	19	17	63	16	53*, 55*	1.2, 1.3
D	0.26	295	26	3	24	72	15	51*, 50*	1.1, 1.0
7	0.06	157	16	29	62	9	31	-	-
E	0.34	324	23	43	32	25	23	52*, 52*, 93	1.1, 1.1, 7.5
8	0.39	366	15	75	23	1	39	-	-
9	0.15	132	11	86	12	1	49	-	-
10	0.2	322	17	85	15	0	47	-	-
11	0.12	116	8	96	4	0	54	-	-
12	0.67	357	21	85	8	0	52	93	7.5

Table 3: Summary of watershed characteristics and rainfall intensities that produced debris flows. The 15-minute rainfall intensity threshold predicted by the M1 likelihood model is denoted by I_{15}^{M1} while I_{15} denotes the 15-minute rainfall intensity associated with debris flow initiation. An asterisk indicates a constraint on debris flow timing within the rainstorm, meaning that I_{15} denotes the triggering intensity. RI is the recurrence interval of I_{15} .

Watersheds that produced debris flows were characterized by mean slopes greater than 20 degrees and a fraction of area burned at moderate or high severity that exceeded 0.57 in all but one instance (Table 3). Watershed 12, only 8% of which burned at moderate or high severity, produced a debris flow. Watersheds with substantial area burned at moderate or high severity, such as watershed 7 with 71% area burned at moderate/high severity, did not always produce debris flows if they had a more modest mean slope. The I_{15} thresholds determined by the M1 model, however, account for spatially variable terrain and burn severity properties among watersheds that affect debris flow potential. The M1 modelled I_{15} thresholds, I_{15}^{M1} , varied from 16 mm/h to



54 mm/h. Since all watersheds shared the same average soil KF factor, 0.2, variations in the modelled thresholds can be attributed to differences in topography, soil burn severity classification, and $dNBR$. Ten watersheds had $I_{15}^{M1} \leq 25$ mm/h, and all of these watersheds produced debris flows (Table 3). Watershed 12 also produced a debris flow despite having the second highest M1 threshold of all monitored watersheds, $I_{15}^{M1} = 52$ mm/h.



520 **Figure 6:** (a) Ternary diagram showing differences in the fractions of sand, silt, and clay within the fine (< 2 mm) fraction of samples from debris flow deposits and burned hillslopes. Debris flow deposits have, on average, substantially greater sand content. (b) Grain size distributions of the coarse fraction (> 2 mm) from two debris flow deposits as determined by a pebble count. A total of 86 and 158 clasts were counted for the deposits in watershed A and D, respectively.

4.3 Characteristics of debris flow-triggering rainstorms

We were able to determine debris flow timing within rainstorms for nine of the 16 observed debris flows based on time series data from pressure transducers (Figure 7) and geophones (Figure 8). Six debris flows occurred in watersheds that were not intensively monitored. Two debris flows initiated in watershed A, where geophones were installed, during rainstorms on 24 July 2020 and 9 September 2020. Seven debris flow events were captured by pressure transducers. The one remaining debris flow occurred on 9 September 2020 in watershed E, but we were unable to get timing information for this flow since the pressure transducer was destroyed by a debris flow on 21 July 2020. The peak 15-minute rainfall intensities of rainstorms that produced debris flows, all of which occurred in the first few months following the fire, varied from 34-93 mm/h (Table 3). Peak 15-minute rainfall intensities were lower during the 2021 and 2022 monsoon season, but the lowest debris flow-triggering rainfall intensity of $I_{15}=33$ mm/h was exceeded during 4 rainstorms in 2021 and 3 rainstorms in 2022. The highest I_{15} recorded after the 2020 monsoon season, $I_{15}=56$ mm/h, occurred on 15 August 2022.



In the nine cases where we were able to determine debris flow timing within rainstorms, we computed the triggering I_{15} and found that it ranged from 33-76 mm/h (Table 3). In four of the nine cases, the peak and triggering I_{15} were the same. In the five remaining cases, the difference between the peak and triggering I_{15} was 43, 38, 1, 2, and 10 mm/h (Table S2). Storm cumulative rainfall totals were also greater than storm rainfall totals prior to debris flows, with the most substantial difference (31 mm) occurring during the storm on 9 September 2020 (Table S2). On average, the debris flow triggering time (i.e., the time the debris flow was observed at the outlet) was approximately 3 minutes after the time of the peak I_{15} . There was an average of less than 1 minute between the debris flow triggering time and the time of peak I_{10} . In contrast, debris flow triggering times preceded the time of peak I_{30} and I_{60} by roughly 13 and 31 minutes.

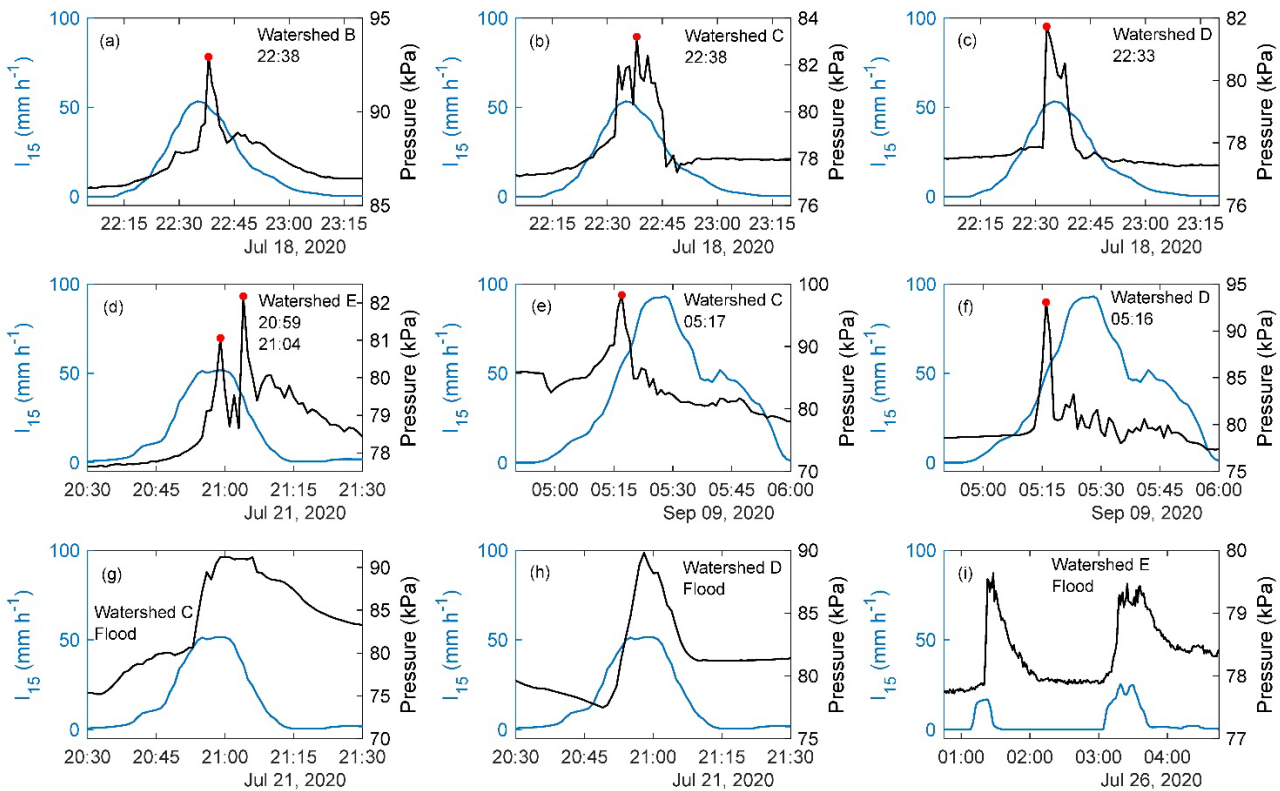
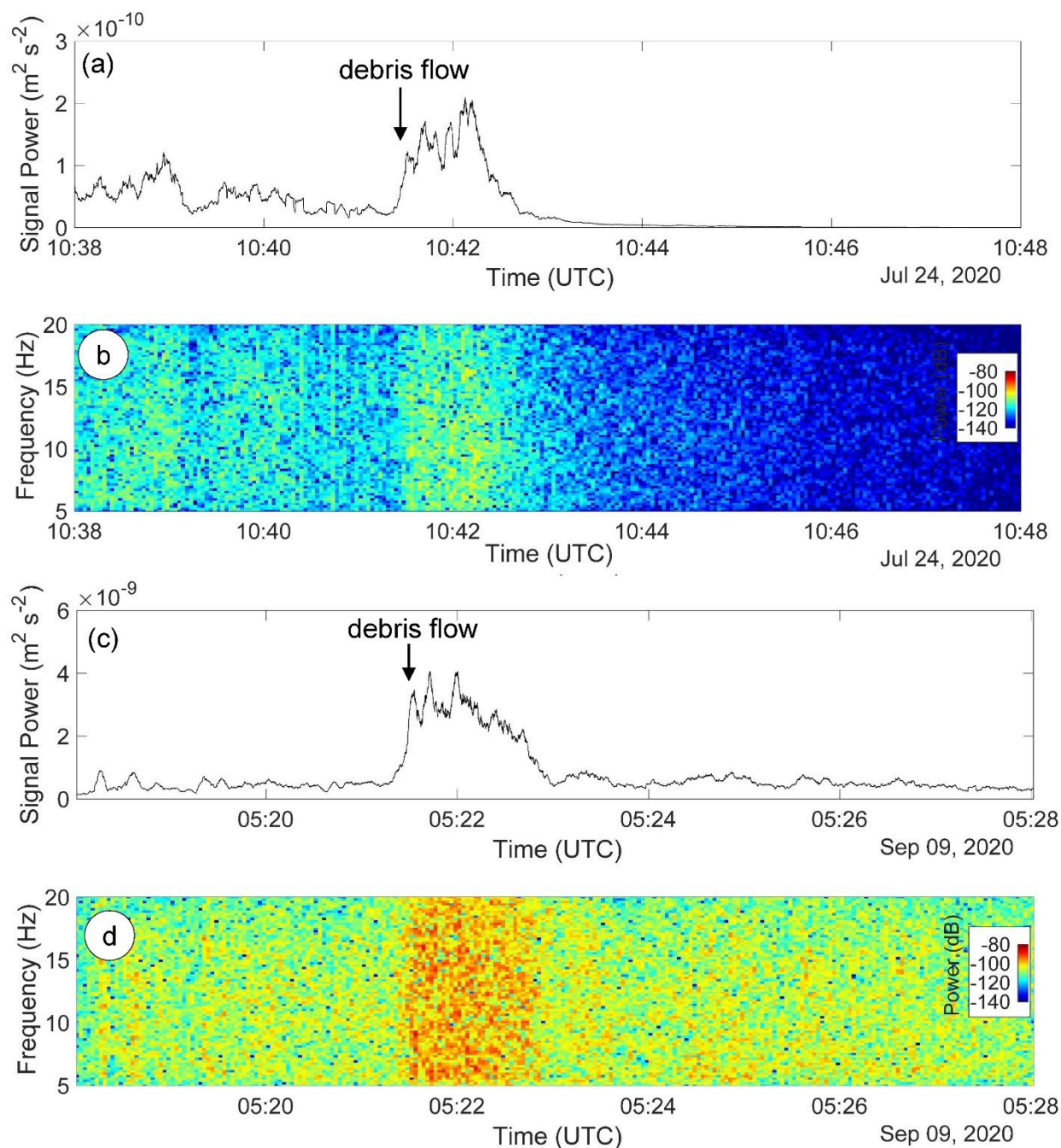


Figure 7: We determined timing of debris flows during rainstorms based on rapid changes in pressure over time periods of several minutes. (a-f) The timing of a debris flow is indicated by a red dot, with the time (UTC) included in the upper right corner. (g-i) Water-dominated flood flows are characterized by a more gradual rise and fall of pressure that roughly coincides with temporal variations in the 15-minute average rainfall intensity, I_{15} .

Debris flow-producing rainstorms could be separated reasonably well from those that did not produce debris flows by using an ID threshold (Figure 9). The threshold intensities associated with durations of 5, 10, 15, 30, and 60 minutes are 85, 52, 39, 26, and 15 mm/h, respectively. The performance of the thresholds varied with duration. Threat scores of 0.43, 0.41, 0.41, 0.38,



and 0.35 were associated with durations of 5, 10, 15, 30, and 60 minutes, which indicates better performance when using intensities averaged over shorter durations.

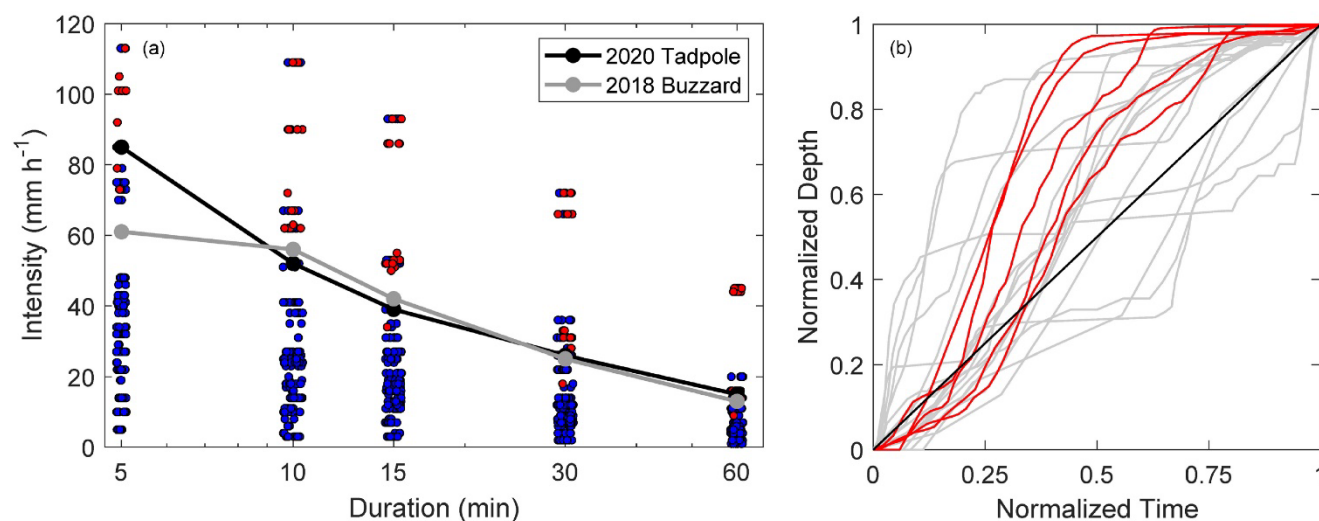


555 **Figure 8:** We used ground velocity recorded by the upper geophone to estimate debris flows timing within rainstorms at watershed A on (a,b) 24 July 2020 and (c,d) 9 Sept 2020. Passage of a debris flow is characterized by a rapid increase in signal power (dB), which tapers off more slowly, across a range of frequencies.



560 The recurrence interval of peak 15-minute rainfall intensities during debris flow-producing storms ranged from 0.5-7.5 years with a mean of 3.4 years. In contrast, the recurrence interval of 15-minute rainfall intensities that triggered debris flows (i.e., only including observations where we have flow timing data) ranged from 0.5-3.4 years with a mean of 1.3 years (Table 3). All four rainstorms that produced debris flows were categorized as Q2 storms since more rainfall occurred during the second quartile of the storm duration than during any of the three other quartiles. There was a total of 24 remaining rainfall records with a peak I_{15} above 10 mm/h and 6, 6, 4, and 8 of these were categorized as Q1, Q2, Q3, and Q4, respectively. The four debris flow-triggering rainstorms all share qualitatively similar SRP patterns but are not extreme in terms of their rainfall distributions relative to other rainstorms that did not produce debris flows (Figure 9).

565



570 **Figure 9:** (a) Rainstorms that produced debris flows (red circles) can be separated well in intensity-duration (ID) space from those that produced flood responses or no response (blue circles). The rainfall ID threshold derived for the Tadpole Fire is similar to the threshold derived previously by McGuire and Youberg (2020) for the nearby 2018 Buzzard Fire. (b) The temporal distribution of rainfall within rainstorms that produced debris flows (red lines) are similar, with the majority of rainfall occurring during the second quarter of the storm duration ($0.25 \leq \text{normalized time} \leq 0.5$). Rainstorms that did not produce debris flows (grey lines) are characterized by more varied distributions of rainfall.

5 Discussion

575 5.1 Spatial and temporal patterns in debris flow activity

The first debris flows following the fire initiated on 18 July 2020, roughly 6 weeks after the fire ignited on 6 June 2020 and only two days after the fire was contained on 16 July 2020. It is not uncommon in the southwestern USA, particularly in Arizona and New Mexico, for post-fire debris flows to initiate shortly following, or even prior to, fire containment. Debris flows initiated at the Pinal (Raymond et al., 2020) and Frye Fires (McGuire and Youberg, 2019) in southern Arizona in July



580 2017 prior to when each was contained, in August and September 2017, respectively. The potentially short time between fire
containment and the onset of intense monsoon rainfall capable of triggering debris flows highlights the importance of pre-fire
planning for post-fire hazards in this region (Tillery et al., 2014). In terms of the temporal persistence of the debris flow hazard,
our study site experienced a marked reduction in PFDF susceptibility over a time of one year or less, with no debris flows
occurring during the second or third monsoon season after the fire. DeGraff (2015) found that roughly 71% of post-fire debris
585 flows were generated in the first 6 months following fire, though Hoch et al. (2021) and Tillery and Rengers (2020) reported
runoff generated debris flows 1-2 years following fire in ponderosa pine forests of western New Mexico.

Examining the temporal changes in understory vegetation, ground cover, and soil hydraulic properties in relation to changes
in debris flow activity provide insight into the fire-related factors controlling PFDF initiation. All of the observed debris flows
590 occurred within the first two months following containment of the fire in July 2020 (Table 3). The highest peak I_{15} at the
watershed A rain gage occurred during the first monsoon season. However, peak I_{15} exceeded 33 mm/h, which was the lowest
 I_{15} that led to a debris flow response, in subsequent monsoon seasons, including during 4 storms in 2021 and 3 storms during
2022 compared with 3 storms during 2020 (Figure S3). Therefore, we do not attribute the observed decline in debris flow
activity over time to reductions in rainfall intensity. We documented temporal changes in soil hydraulic properties following
595 fire that exhibit variations around those measured in nearby unburned soils (Figure 4), which demonstrates these soil hydraulic
properties were relatively resistant to change following the Tadpole Fire. In contrast, the marked decrease in debris flow
activity over time coincided with a consistent decrease in bare ground in areas burned at moderate/high severity (Table 1). Past
studies in forested environments, in particular, have demonstrated the importance of litter and duff layers in controlling
infiltration, runoff, and erosion (Neris et al., 2013). Loss of litter and duff and the subsequent exposure of bare ground can lead
600 to substantial increases in runoff and erosion, even in the absence of burning (Robichaud et al., 2016). Due to the close link
between runoff, erosion, and PFDF initiation at our site, we hypothesize that the loss of litter and duff played a key role in
increasing debris flow likelihood. We cannot rule out, however, additional controls on debris flow activity from other potential
fire-related changes to soil physical properties that were not measured, such as aggregate stability, organic matter, and apparent
cohesion associated with fine roots.

605
Infiltration measurements with minidisk infiltrometers did not demonstrate strong spatial differences in soil hydraulic
properties with respect to burn severity. Following the Tadpole Fire, we estimated similar values of K_{fs} , S , and h_f in areas
burned at moderate/high severity relative to unburned areas or areas burned at low severity (Figure 4, Table 2). Infiltration
modelling further demonstrates that, across a range of rainfall intensities, runoff ratios and peak runoff rates would be slightly
610 greater in areas burned at moderate/high severity relative to unburned soils and soils burned at low severity when interception
and other potential forms of water storage (i.e., by litter, duff) are neglected (Figure 5). Despite these trends, we only observed
runoff-generated debris flows in watersheds that contained a substantial fraction of area burned at moderate/high severity, with
one exception. These results support the hypothesis that factors other than fire-induced changes to infiltration capacity, namely



615 decreases in canopy and ground cover (Table 1), were first-order controls on lowering debris flow initiation thresholds in
watersheds burned at moderate and high severity. A number of studies at small scales indicate that ground cover is an important
control on post-fire sediment yield (Benavides-Solorio and MacDonald, 2001; Robichaud et al., 2013; Johansen et al., 2001).
Increases in bare ground are associated with decreased interception, lower hydraulic roughness, and increases in rilling and
raindrop-induced erosion on hillslopes that make it easier to mobilize the volume of sediment required to initiate runoff-
generated PFDFs (Meyer and Wells, 1997; Larsen et al., 2009).

620

Variations in rainfall ID thresholds from one watershed to another, which we expect based on differences in watershed
morphology and burn severity characteristics, may be accounted for using the M1 likelihood model to estimate basin specific
rainfall ID thresholds (Staley et al., 2017). The M1 likelihood model, which was trained using observations from southern
California, underpredicted rainfall thresholds for debris flow initiation at the Tadpole Fire (Table 3). However, the M1 model
625 performed well at identifying the monitored watersheds that were most susceptible to debris flows. The watersheds with the
lowest M1 I_{15} threshold were also the watersheds that produced debris flows whereas those with higher thresholds did not
produce debris flows (Table 3). The lone exception to this trend is watershed 12. Watershed 12 was located farthest from the
rain gages (4.1 km), so it is possible that the debris flow observed there was triggered by more intense rainfall than what was
received by the rain gages and the other watersheds (Figure 1). The ability of the M1 model to assess relative susceptibility
630 indicates that the variables in the M1 model, namely $MH23$, $dNBR$, and soil KF factor, remain good predictors of debris flow
potential in our study area despite the previously noted site specific differences (e.g., presence/absence of dry ravel) in debris
flow initiation processes between southern California and our study site. A study of runoff-generated post-fire debris flows in
Greece also recently found a significant correlation between debris flow occurrence and a debris flow likelihood predicted by
a slightly modified version of the M1 model (Diakakis et al., 2023), which used a Europe-wide soil erodibility index (K-factor)
635 (Panagos et al., 2014) in place of the KF factor. The model's ability to identify watersheds susceptible to debris flows across
these different settings suggests that it captures elements of watershed morphology that are first-order controls on debris flow
initiation.

5.2 Characteristics of debris flow triggering rainstorms

The 15-minute average rainfall intensities responsible for triggering debris flows ranged from 33-76 mm/h (Table 3). These
640 rainfall intensities are greater than the $I_{15}=19$ mm/h threshold for PFDFs in the San Gabriel Mountains of southern California
(Staley et al., 2013), but are consistent with other recent observations from western New Mexico where the triggering I_{15} varied
from 28-79 mm/h (McGuire and Youberg, 2020). The recurrence interval of I_{15} that produced debris flows at the Tadpole Fire,
which had a mean of 1.3 years when considering only cases where we have constraints on debris flow timing within rainstorms,
highlights the susceptibility of severely burned watersheds to debris flows. Staley et al. (2020) similarly found that the RI of
645 debris flow-producing I_{15} across a range of burned sites in the western USA had a geometric mean of 0.9 years.



A comparison of the rainfall ID thresholds between the Tadpole Fire and the nearby 2018 Buzzard Fire, which also burned through ponderosa-pine in the Gila National Forest, indicates similarities that are encouraging for application of a regional PDFD ID threshold for similar areas in New Mexico (Figure 9). The I_{15} threshold of 39 mm/h is roughly equivalent to the 42 mm/h threshold found at the Buzzard Fire (McGuire and Youberg, 2020) and slightly lower than the 56 mm/h threshold identified by Raymond et al. (2020) following fire in chaparral-dominated watersheds in southern Arizona. A comparison of the Tadpole Fire I_{15} threshold (39 mm/h) with the regional threshold for the San Gabriel Mountains (19 mm/h) (Staley et al., 2013), however, indicates that more intense rainstorms are generally needed to trigger debris flows via runoff in the immediate aftermath of fire in forested steepplands in New Mexico relative to southern California. These differences could be associated with variations in watershed morphology among the two locations (e.g., slope, channel width), sediment availability (e.g., relatively minimal dry ravel activity in New Mexico), or to differences in the typical severity or spatial patterns of burn severity. However, it appears that these are not the only factors involved since variations in watershed morphology and burn severity that are first order controls on debris flow likelihood should be accounted for by the M1 model.

The M1 modelled I_{15} thresholds substantially underestimated the I_{15} needed to trigger debris flows in our study area. The average difference between the triggering I_{15} and the M1 modelled I_{15} threshold, in watersheds where we could constrain debris flow timing within rainstorms, was 36 mm/h (Table 3). We hypothesize that a bias towards underestimating ID thresholds at our site may be related, at least in part, to differences in the climatology of intense rainfall between our study site and the sites in southern California that supplied the training data for the M1 model and/or to differences in the particle size distribution and cohesion of sediment available for transport following fire. We did not observe dry ravel at our site and the main sediment source for debris flows appeared to be colluvial deposits stored in unincised valley bottoms. This is in strong contrast to the abundant supply of fine, relatively cohesionless sediment delivered from hillslopes to channels via dry ravel following fire in the San Gabriel Mountains (DiBiase and Lamb, 2020).

Rainfall ID thresholds and estimates of the RI of rainfall associated with debris flow initiation provide information for practitioners, decision-makers, and emergency managers tasked with assessing and mitigating the effects of PDFD hazards. There is a general gap, however, in the data that constrain the timing of debris flows within rainstorms in many regions (Staley et al., 2020). In the absence of in-situ monitoring equipment, such as stage gauges, pressure transducers, geophones, or video cameras, the peak rainfall intensity during a debris flow-producing storm is taken as an estimate of the triggering intensity. Staley et al. (2013) document significant differences between triggering intensities and peak intensities in southern California and data from Raymond et al. (2020) indicate that 15-minute peak intensities overestimate debris flow-triggering intensities, on average, by 26 mm/h in southern Arizona. Here, differences between peak and triggering I_{15} varied from 0-43 mm/h. If peak rainfall intensity were used in all cases to estimate the triggering I_{15} , the average RI of the debris flow-triggering I_{15} would increase from 1.3 to 3.4 years. The observations presented here help improve situational awareness for PDFDs in a region



680 where increases in the number of fires and area burned at high severity (Singleton et al., 2019) are likely to promote conditions conducive to larger and more frequent debris flows.

6 Conclusion

We monitored debris flow activity in a series of steep watersheds burned by the 2020 Tadpole Fire in western New Mexico, USA over more than two years. Sixteen debris flows initiated within 11 different watersheds in the first monsoon season following the fire. Rainfall intensities responsible for triggering debris flows were not extreme, having recurrence intervals of approximately 1 year. No debris flows were observed during the second or third monsoon season following fire, despite rainfall intensities that exceeded those responsible for triggering debris flows in the first several months after the fire. These observations indicate a rapid reduction in debris flow susceptibility with time since fire. Measurements of soil infiltration, understory canopy cover, and ground cover indicate that post-fire changes to soil hydraulic properties did not play a primary role in promoting debris flow initiation following the fire. Fifteen of the sixteen debris flows initiated in watersheds that burned primarily at moderate or high severity. However, in-situ measurements indicated similar or slightly greater soil infiltration capacity immediately following fire in areas burned at moderate to high severity relative to areas that were unburned or burned at low severity. We attribute increased debris flow activity in areas burned at moderate to high severity to decreases in canopy and ground cover, which were substantially lower immediately following the fire in areas burned at moderate to high severity compared with areas burned at low severity. Although we note many differences between our study area and recently burned areas in southern California, a debris flow likelihood model trained on data from southern California was successful at providing a relative measure of debris flow susceptibility across our monitored watersheds. Results provide additional constraints on the rainfall intensities responsible for triggering PFDFs in a region where increases in the number of fires and the area burned at high severity are anticipated to increase risk associated with PFDFs in the future.

700

Data availability: Data used for analyses in this study are available in McGuire et al. (2023) and Rengers et al. (2022).

Author contributions: McGuire, Rengers, Youberg, Gorr, and Hoch planned the study and performed initial field equipment installation. McGuire, Rengers, Youberg, Gorr, Hoch, and Beers maintained field equipment and contributed to field data collection efforts. Porter led analysis of the geophone data. McGuire prepared the manuscript and led other data analysis tasks with contributions from all co-authors.

705

Competing Interests: The authors declare that they have no conflict of interest.



710 *Acknowledgements:* Any use of trade, firm, or product names is for descriptive purposes only and does not imply endorsement by the U.S. Government. This research was supported by the National Integrated Drought Information System (NIDIS) (task order no. 1332KP20FNRMT0012) and the U.S. Geological Survey Landslide Hazards Program.

References

- Benavides-Solorio, J. and MacDonald, L. H.: Post-fire runoff and erosion from simulated rainfall on small plots, Colorado Front Range, *Hydrol Process*, 15, 2931–2952, 2001.
- Bonnin, G. M., Martin, D., Lin, B., Parzybok, T., Yekta, M., and Riley, D.: NOAA Atlas 14, Precipitation-Frequency Atlas of the United States, Volume 1 Version 5.0: Semiarid Southwest (Arizona, Southeast California, Nevada, New Mexico, Utah), Silver Spring, MD, 2011.
- Bunte, K. and Abt, S. R.: Sampling Surface and Subsurface Particle-Size Distributions in Wadable Gravel- and Cobble-Bed Streams for Analyses in Sediment Transport, Hydraulics, and Streambed Monitoring, General Technical Report RMRS-GTR-74, 450 pp., 2001.
- 720 Cannon, S. H., Gartner, J. E., Wilson, R. C., Bowers, J. C., and Laber, J. L.: Storm rainfall conditions for floods and debris flows from recently burned areas in southwestern Colorado and southern California, *Geomorphology*, 96, 250–269, 2008.
- Cannon, S. H., Gartner, J. E., Rupert, M. G., Michael, J. A., Rea, A. H., and Parrett, C.: Predicting the probability and volume of postwildfire debris flows in the intermountain western United States, *Geol Soc Am Bull*, 122, 127–144, 2010.
- 725 Carsel, R. F. and Parrish, R. S.: Developing joint probability distributions of soil water retention characteristics, *Water Resour Res*, 24, 755–769, 1988.
- Conedera, M., Peter, L., Marxer, P., Forster, F., Rickenmann, D., and Re, L.: Consequences of forest fires on the hydrogeological response of mountain catchments: a case study of the Riale Buffaga, Ticino, Switzerland, *Earth Surf Process Landf*, 28, 117–129, <https://doi.org/10.1002/esp.425>, 2003.
- 730 Costa, J. E.: Rheologic, geomorphic, and sedimentologic differentiation of water floods, hyperconcentrated flows, and debris flows, *Flood Geomorphology*. John Wiley & Sons New York. 1988. p 113-122., 1988.
- Crocker, R. L. and Tiver, N. S.: Survey methods in grassland ecology, *Grass and Forage Science*, 3, 1–26, 1948.
- Degraff, J. V., Cannon, S. H., and Gartner, J. E.: The Timing of Susceptibility to Post-Fire Debris Flows in the Western United States, *Environmental & Engineering Geoscience*, 21, 277–292, 2015.
- 735 Diakakis, M., Mavroulis, S., Vassilakis, E., and Chalvatzi, V.: Exploring the Application of a Debris Flow Likelihood Regression Model in Mediterranean Post-Fire Environments, Using Field Observations-Based Validation, *Land (Basel)*, 12, 555, <https://doi.org/10.3390/land12030555>, 2023.
- DiBiase, R. A. and Lamb, M. P.: Dry sediment loading of headwater channels fuels post-wildfire debris flows in bedrock landscapes, *Geology*, 48, 189–193, <https://doi.org/10.1130/G46847.1>, 2020.
- 740



- Ebel, B. A.: Temporal evolution of measured and simulated infiltration following wildfire in the Colorado Front Range, USA: Shifting thresholds of runoff generation and hydrologic hazards, *J Hydrol (Amst)*, 585, 124765, <https://doi.org/10.1016/j.jhydrol.2020.124765>, 2020.
- Ebel, B. A. and Martin, D. A.: Meta-analysis of field-saturated hydraulic conductivity recovery following wildland fire: Applications for hydrologic model parameterization and resilience assessment, *Hydrol Process*, 31, 3682–3696, <https://doi.org/10.1002/hyp.11288>, 2017.
- Ebel, B. A. and Moody, J. A.: Synthesis of soil-hydraulic properties and infiltration timescales in wildfire-affected soils, *Hydrol Process*, 31, 324–340, <https://doi.org/10.1002/hyp.10998>, 2017.
- Ebel, B. A., Moody, J. A., and Martin, D. A.: Post-fire temporal trends in soil-physical and -hydraulic properties and simulated runoff generation: Insights from different burn severities in the 2013 Black Forest Fire, CO, USA, *Science of the Total Environment*, 802, <https://doi.org/10.1016/j.scitotenv.2021.149847>, 2022.
- Esposito, G., Gariano, S. L., Masi, R., Alfano, S., and Giannatiempo, G.: Rainfall conditions leading to runoff-initiated post-fire debris flows in Campania, Southern Italy, *Geomorphology*, 423, <https://doi.org/10.1016/j.geomorph.2022.108557>, 2023.
- Florsheim, J. L., Keller, E. A., and Best, D. W.: Fluvial sediment transport in response to moderate storm flows following chaparral wildfire, Ventura County, southern California, *Geol Soc Am Bull*, 103, 504–511, [https://doi.org/10.1130/0016-7606\(1991\)103<0504:FSTIRT>2.3.CO;2](https://doi.org/10.1130/0016-7606(1991)103<0504:FSTIRT>2.3.CO;2), 1991.
- Friedman, E. Q. and Santi, P. M.: Relationship between rainfall intensity and debris-flow initiation in a southern Colorado burned area, in: *Association of Environmental and Engineering Geologists Special Publication 28*, 2019.
- Gabet, E. J. and Bookter, A.: A morphometric analysis of gullies scoured by post-fire progressively bulked debris flows in southwest Montana, USA, *Geomorphology*, 96, 298–309, 2008.
- García-Ruiz, J. M., Arnáez, J., Gómez-Villar, A., Ortigosa, L., and Lana-Renault, N.: Fire-related debris flows in the Iberian Range, Spain, *Geomorphology*, 196, 221–230, <https://doi.org/10.1016/j.geomorph.2012.03.032>, 2013.
- Green, H. W. and Ampt, G. A.: Studies on Soil Physics, 1. The flow of air and water through soils, *J Agric Sci*, 4, 1–24, 1911.
- Hoch, O. J., McGuire, L. A., Youberg, A. M., and Rengers, F. K.: Hydrogeomorphic Recovery and Temporal Changes in Rainfall Thresholds for Debris Flows Following Wildfire, *J Geophys Res Earth Surf*, 126, <https://doi.org/10.1029/2021JF006374>, 2021.
- Holden, Z. A., Swanson, A., Luce, C. H., Jolly, W. M., Maneta, M., Oyler, J. W., Warren, D. A., Parsons, R., and Affleck, D.: Decreasing fire season precipitation increased recent western US forest wildfire activity, *Proc Natl Acad Sci U S A*, 115, E8349–E8357, <https://doi.org/10.1073/pnas.1802316115>, 2018.
- Huff, F. A.: Time distribution of rainfall in heavy storms, *Water Resour Res*, 3, 1007–1019, <https://doi.org/10.1029/WR003i004p01007>, 1967.
- Johansen, M. P., Hakonson, T. E., and Breshears, D. D.: Post-fire runoff and erosion from rainfall simulation: contrasting forests with shrublands and grasslands, *Hydrol Process*, 15, 2953–2965, 2001.



- Kean, J. W., Staley, D. M., and Cannon, S. H.: In situ measurements of post-fire debris flows in southern California: Comparisons of the timing and magnitude of 24 debris-flow events with rainfall and soil moisture conditions, *Journal of Geophysical Research: Earth Surface* (2003--2012), 116, 1–21, <https://doi.org/10.1029/2011JF002005>, 2011.
- Kean, J. W., Staley, D. M., Leeper, R. J., Schmidt, K. M., and Gartner, J. E.: A low-cost method to measure the timing of postfire flash floods and debris flows relative to rainfall, *Water Resour Res*, 48, 2012.
- Kean, J. W., Coe, J. A., Coviello, V., Smith, J. B., McCoy, S. W., and Arattano, M.: Estimating rates of debris flow entrainment from ground vibrations, *Geophys Res Lett*, 42, 6365–6372, <https://doi.org/10.1002/2015GL064811>, 2015.
- Kean, J. W., McGuire, L. A., Rengers, F. K., Smith, J. B., and Staley, D. M.: Amplification of postwildfire peak flow by debris, *Geophys Res Lett*, 43, <https://doi.org/10.1002/2016GL069661>, 2016.
- Kean, J. W., Staley, D. M., Lancaster, J. T., Rengers, F. K., Swanson, B. J., Coe, J. A., Hernandez, J. L., Sigman, A. J., Allstadt, K. E., and Lindsay, D. N.: Inundation, flow dynamics, and damage in the 9 January 2018 Montecito debris-flow event, California, USA: Opportunities and challenges for post-wildfire risk assessment, *Geosphere*, 15, 1140–1163, <https://doi.org/10.1130/GES02048.1>, 2019.
- Kern, A. N., Addison, P., Oommen, T., Salazar, S. E., and Coffman, R. A.: Machine Learning Based Predictive Modeling of Debris Flow Probability Following Wildfire in the Intermountain Western United States, *Math Geosci*, 49, 717–735, <https://doi.org/10.1007/s11004-017-9681-2>, 2017.
- Kirchmeier-Young, M. C. and Zhang, X.: Human influence has intensified extreme precipitation in North America, *Proceedings of the National Academy of Sciences*, 117, 13308–13313, <https://doi.org/10.1073/pnas.1921628117/-DCSupplemental.y>, 2020.
- Lamb, M. P., Scheingross, J. S., Amidon, W. H., Swanson, E., and Limaye, A.: A model for fire-induced sediment yield by dry ravel in steep landscapes., *J Geophys Res*, 116, 2011.
- Lancaster, J. T., Swanson, B. J., Lukashov, S. G., Oakley, N. S., Lee, J. B., Spangler, E. R., Hernandez Brian P E Olson Mike J Defrisco, J. L., Lindsay, D. N., Schwartz, Y. J., and Mccrea Peter D Roffers Christopher M Tran, S. E.: Observations and Analyses of the 9 January 2018 Debris-Flow Disaster, Santa Barbara County, California, *Environmental & Engineering Geoscience*, 3–27 pp., 2021.
- Langhans, C., Smith, H. G., Chong, D. M. O., Nyman, P., Lane, P. N. J., and Sheridan, G. J.: A model for assessing water quality risk in catchments prone to wildfire, *J Hydrol (Amst)*, 534, 407–426, <https://doi.org/10.1016/j.jhydrol.2015.12.048>, 2016.
- Larsen, I. J., Pederson, J. L., and Schmidt, J. C.: Geologic versus wildfire controls on hillslope processes and debris flow initiation in the Green River canyons of Dinosaur National Monument, *Geomorphology*, 81, 114–127, <https://doi.org/10.1016/j.geomorph.2006.04.002>, 2006.
- Larsen, I. J., MacDonald, L. H., Brown, E., Rough, D., Welsh, M. J., Pietraszek, J. H., Libohova, Z., de Dios Benavides-Solorio, J., and Schaffrath, K.: Causes of post-fire runoff and erosion: water repellency, cover, or soil sealing?, *Soil Science Society of America Journal*, 73, 1393–1407, 2009.



- Liu, T., McGuire, L. A., Youberg, A. M., Gorr, A. N., and Rengers, F. K.: Guidance for parameterizing post-fire hydrologic models with in situ infiltration measurements, *Earth Surf Process Landf*, <https://doi.org/10.1002/esp.5633>, 2023.
- 810 McGuire, L. A. and Youberg, A. M.: Impacts of successive wildfire on soil hydraulic properties: Implications for debris flow hazards and system resilience, *Earth Surf Process Landf*, 44, <https://doi.org/10.1002/esp.4632>, 2019.
- McGuire, L. A. and Youberg, A. M.: What drives spatial variability in rainfall intensity-duration thresholds for post-wildfire debris flows? Insights from the 2018 Buzzard Fire, NM, USA, *Landslides*, 17, 2385–2399, <https://doi.org/10.1007/s10346-020-01470-y>, 2020.
- 815 McGuire, L. A., Kean, J. W., Staley, D. M., Rengers, F. K., and Wasklewicz, T. A.: Constraining the relative importance of raindrop- and flow-driven sediment transport mechanisms in postwildfire environments and implications for recovery time scales, *J Geophys Res Earth Surf*, 121, <https://doi.org/10.1002/2016JF003867>, 2016.
- McGuire, L. A., Rengers, F. K., Kean, J. W., Staley, D. M., and Mirus, B. B.: Incorporating spatially heterogeneous infiltration capacity into hydrologic models with applications for simulating post-wildfire debris flow initiation, *Hydrol Process*, 32, 1173–
820 1187, <https://doi.org/10.1002/hyp.11458>, 2018.
- McGuire, L. A., Youberg, A. M., Rengers, F. K., Abramson, N. S., Ganesh, I., Gorr, A. N., Hoch, O., Johnson, J. C., Lamom, P., Prescott, A. B., Zanetell, J., and Fenerty, B.: Extreme Precipitation Across Adjacent Burned and Unburned Watersheds Reveals Impacts of Low Severity Wildfire on Debris-Flow Processes, *J Geophys Res Earth Surf*, 1–21, <https://doi.org/10.1029/2020jf005997>, 2021.
- 825 McGuire, L. A., F. K. Rengers, A. M. Youberg, A. N. Gorr, O. Hoch, and R. Beers: Hydrologic monitoring and field data collected following the 2020 Tadpole Fire, New Mexico, USA, *HydroShare*, <http://www.hydroshare.org/resource/136ecec98a4141e6aedb57bdf6fb1fb5>, 2023.
- Meyer, G. A. and Wells, S. G.: Fire-related sedimentation events on alluvial fans, Yellowstone National Park, USA, *Journal of Sedimentary Research*, 67, 776–791, 1997.
- 830 Miller, J. D. and Thode, A. E.: Quantifying burn severity in a heterogeneous landscape with a relative version of the delta Normalized Burn Ratio (dNBR), *Remote Sens Environ*, 109, 66–80, <https://doi.org/10.1016/j.rse.2006.12.006>, 2007.
- Moody, J. A., Smith, J. D., and Ragan, B. W.: Critical shear stress for erosion of cohesive soils subjected to temperatures typical of wildfires, *J Geophys Res Earth Surf*, 110, <https://doi.org/10.1029/2004JF000141>, 2005.
- Moody, J. A., Ebel, B. A., Nyman, P., Martin, D. A., Stoof, C., and McKinley, R.: Relations between soil hydraulic properties
835 and burn severity, *Int J Wildland Fire*, 25, 279–293, <https://doi.org/10.1071/WF14062>, 2016.
- Neris, J., Tejedor, M., Rodríguez, M., Fuentes, J., and Jiménez, C.: Effect of forest floor characteristics on water repellency, infiltration, runoff and soil loss in Andisols of Tenerife (Canary Islands, Spain), *Catena (Amst)*, 108, 50–57, <https://doi.org/10.1016/j.catena.2012.04.011>, 2013.
- Nikolopoulos, E. I., Destro, E., Abul Ehsan Bhuiyan, M., Borga, M., and Anagnostou, E. N.: Evaluation of predictive models
840 for post-fire debris flow occurrence in the western United States, *Natural Hazards and Earth System Sciences*, 18, 2331–2343, <https://doi.org/10.5194/nhess-18-2331-2018>, 2018.



- Nyman, P., Sheridan, G., Smith, H. G., and Lane, P. N. J.: Evidence of debris flow occurrence after wildfire in upland catchments of south-east Australia, *Geomorphology*, 125, 383–401, 2011.
- Oakley, N. S., Lancaster, J. T., Kaplan, M. L., and Ralph, F. M.: Synoptic conditions associated with cool season post-fire debris flows in the Transverse Ranges of southern California, *Natural Hazards*, 88, 327–354, <https://doi.org/10.1007/s11069-017-2867-6>, 2017.
- Palucis, M. C., Ulizio, T. P., and Lamb, M. P.: Debris Flow Initiation From Ravel-Filled Channel Bed Failure Following Wildfire In A Bedrock Landscape With Limited Sediment Supply, *Bulletin of the Geological Society of America*, 133, 2079–2096, <https://doi.org/10.1130/B35822.1>, 2021.
- 850 Panagos, P., Meusburger, K., Ballabio, C., Borrelli, P., and Alewell, C.: Soil erodibility in Europe: A high-resolution dataset based on LUCAS, *Science of The Total Environment*, 479–480, 189–200, <https://doi.org/10.1016/j.scitotenv.2014.02.010>, 2014.
- Parsons, A., Robichaud, P. R., Lewis, S. A., Napper, C., and Clark, J. T.: Field guide for mapping post-fire soil burn severity, USDA Forest Service - General Technical Report RMRS-GTR, 1–49, <https://doi.org/10.2737/RMRS-GTR-243>, 2010.
- 855 Peduto, D., Iervolino, L., Esposito, G., Foresta, V., Matano, F., and Masi, R.: Clues of wildfire-induced geotechnical changes in volcanic soils affected by post-fire slope instabilities, *Bulletin of Engineering Geology and the Environment*, 81, <https://doi.org/10.1007/s10064-022-02947-x>, 2022.
- Pierson, T. C.: Distinguishing between Debris Flows and Floods from Field Evidence in Small Watersheds, U.S. Geological Survey Fact Sheet No. 2004-3142, 2005.
- 860 Porter, R., Joyal, T., Beers, R., Loverich, J., LaPlante, A., Spruell, J., Youberg, A., Schenk, E., Robichaud, P. R., and Springer, A. E.: Seismic Monitoring of Post-wildfire Debris Flows Following the 2019 Museum Fire, Arizona, *Front Earth Sci (Lausanne)*, 9, <https://doi.org/10.3389/feart.2021.649938>, 2021.
- Raymond, C. A., McGuire, L. A., Youberg, A. M., Staley, D. M., and Kean, J. W.: Thresholds for post-wildfire debris flows: Insights from the Pinal Fire, Arizona, USA, *Earth Surf Process Landf*, 45, <https://doi.org/10.1002/esp.4805>, 2020.
- 865 Rengers, F. K., McGuire, L. A., Kean, J. W., Staley, D. M., and Hobley, D. E. J.: Model simulations of flood and debris flow timing in steep catchments after wildfire, *Water Resour Res*, 52, 6041–6061, <https://doi.org/10.1002/2015WR018176>, 2016.
- Rengers, F. K., McGuire, L. A., Kean, J. W., Staley, D. M., and Youberg, A. M.: Progress in simplifying hydrologic model parameterization for broad applications to post-wildfire flooding and debris-flow hazards, *Earth Surf Process Landf*, 44, <https://doi.org/10.1002/esp.4697>, 2019.
- 870 Rengers, F. K., McGuire, L. A., Youberg, A. M., Gorr, A. N., Hoch, O., Barnhart, K. R., and Beers, R.: Tadpole fire field measurements following the 8 September 2020 debris flow, Gila National Forest, NM, U.S. Geological Survey data release, <https://doi.org/10.5066/P9I564PP>, 2022.
- Rengers, F. K., McGuire, L. A., Barnhart, K. R., Youberg, A. M., Cadol, D., Gorr, A. N., Hoch, O., Beers, R., and Kean, J. W.: The influence of large woody debris on post-wildfire debris flow sediment storage, *Natural Hazards and Earth System Sciences*, 23, 2075–2088, <https://doi.org/10.5194/nhess-23-2075-2023>, 2023.
- 875



- Robichaud, P. R. and Hungerford, R. D.: Water repellency by laboratory burning of four northern Rocky Mountain forest soils, *J Hydrol (Amst)*, 231, 207–219, 2000.
- Robichaud, P. R., Jordan, P., Lewis, S. A., Ashmun, L. E., Covert, S. A., and Brown, R. E.: Evaluating the effectiveness of wood shred and agricultural straw mulches as a treatment to reduce post-wildfire hillslope erosion in southern British Columbia, Canada, *Geomorphology*, 197, 21–33, 2013.
- 880 Robichaud, P. R., Wagenbrenner, J. W., Pierson, F. B., Spaeth, K. E., Ashmun, L. E., and Moffet, C. A.: Infiltration and interrill erosion rates after a wildfire in western Montana, USA, *Catena (Amst)*, 142, 77–88, 2016.
- Scholle, P. A.: *Geologic Map of New Mexico*, Tech. rep., New Mexico Bureau of Geology and Mineral Resources, 2003.
- Scott, D. F. and van Wyk, D. B.: The effects of wildfire on soil wettability and hydrological behaviour of an afforested catchment, *J Hydrol (Amst)*, 121, 239–256, 1990.
- 885 Singleton, M. P., Thode, A. E., Sánchez Meador, A. J., and Iniguez, J. M.: Increasing trends in high-severity fire in the southwestern USA from 1984 to 2015, *For Ecol Manage*, 433, 709–719, <https://doi.org/10.1016/j.foreco.2018.11.039>, 2019.
- Smith, D. P., Schnieders, J., Marshall, L., Melchor, K., Wolfe, S., Campbell, D., French, A., Randolph, J., Whitaker, M., Klein, J., Steinmetz, C., and Kwan, R.: Influence of a Post-dam Sediment Pulse and Post-fire Debris Flows on Steelhead Spawning Gravel in the Carmel River, California, *Front Earth Sci (Lausanne)*, 9, <https://doi.org/10.3389/feart.2021.802825>, 2021.
- 890 Staley, D. M., Kean, J. W., Cannon, S. H., Schmidt, K. M., and Laber, J. L.: Objective definition of rainfall intensity-duration thresholds for the initiation of post-fire debris flows in southern California, *Landslides*, 10, 547–562, <https://doi.org/10.1007/s10346-012-0341-9>, 2013.
- Staley, D. M., Negri, J. A., Kean, J. W., Laber, J. L., Tillery, A. C., and Youberg, A. M.: Prediction of spatially explicit rainfall intensity--duration thresholds for post-fire debris-flow generation in the western United States, *Geomorphology*, 278, 149–162, 2017.
- 895 Staley, D. M., Kean, J. W., and Rengers, F. K.: The recurrence interval of post-fire debris-flow generating rainfall in the southwestern United States, *Geomorphology*, 370, 107392, <https://doi.org/10.1016/j.geomorph.2020.107392>, 2020.
- Stoof, C. R., Vervoort, R. W., Iwema, J., Elsen, E., Ferreira, A. J. D., and Ritsema, C. J.: Hydrological response of a small catchment burned by experimental fire, *Hydrol Earth Syst Sci*, 16, 267–285, 2012.
- 900 Stoof, C. R., Ferreira, A. J. D., Mol, W., van den Berg, J., de Kort, A., Drooger, S., Slingerland, E. C., Mansholt, A. U., Ferreira, C. S. S., and Ritsema, C. J.: Soil surface changes increase runoff and erosion risk after a low-moderate severity fire, *Geoderma*, 239, 58–67, <https://doi.org/10.1016/j.geoderma.2014.09.020>, 2015.
- Thomas, M. A., Rengers, F. K., Kean, J. W., McGuire, L. A., Staley, D. M., Barnhart, K. R., and Ebel, B. A.: Postwildfire Soil-Hydraulic Recovery and the Persistence of Debris Flow Hazards, *J Geophys Res Earth Surf*, 126, <https://doi.org/10.1029/2021JF006091>, 2021.
- 905 Tillery, Anne C, Haas, Jessica R, Miller, Lara W, Scott, Joe H, Thompson, and Matthew P: Potential Postwildfire Debris-Flow Hazards-A Prewildfire Evaluation for the Sandia and Manzano Mountains and Surrounding Areas, Central New Mexico Scientific Investigations Report 2014-5161, 2014.



- 910 Tillery, A. C. and Matherne, A. M.: Postwildfire debris-flow hazard assessment of the area burned by the 2012 Little Bear fire, south-central New Mexico, U.S. Geological Survey Open-File Report 2013–1108, 2012.
- Tillery, A. C. and Rengers, F. K.: Controls on debris-flow initiation on burned and unburned hillslopes during an exceptional rainstorm in southern New Mexico, USA, *Earth Surf Process Landf*, 45, 1051–1066, <https://doi.org/10.1002/esp.4761>, 2020.
- Vandervaere, J.-P., Vauclin, M., and Elrick, D. E.: Transient flow from tension infiltrometers II. Four methods to determine
915 sorptivity and conductivity, *Soil Science Society of America Journal*, 64, 1272–1284, 2000.
- Vieira, D. C. S., Fernández, C., Vega, J. A., and Keizer, J. J.: Does soil burn severity affect the post-fire runoff and interrill erosion response? A review based on meta-analysis of field rainfall simulation data, *J Hydrol (Amst)*, 523, 452–464, <https://doi.org/10.1016/j.jhydrol.2015.01.071>, 2015.
- Wall, S. A., Roering, J. J., and Rengers, F. K.: Runoff-initiated post-fire debris flow Western Cascades, Oregon, *Landslides*,
920 17, 1649–1661, <https://doi.org/10.1007/s10346-020-01376-9>, 2020.
- Wells, W. G.: The effects of fire on the generation of debris flows in southern California, *Reviews in Engineering Geology*, 7, 105–114, 1987.
- Zhang, R.: Determination of soil sorptivity and hydraulic conductivity from the disk infiltrometer, *Soil Science Society of America Journal*, 61, 1024–1030, 1997.

925